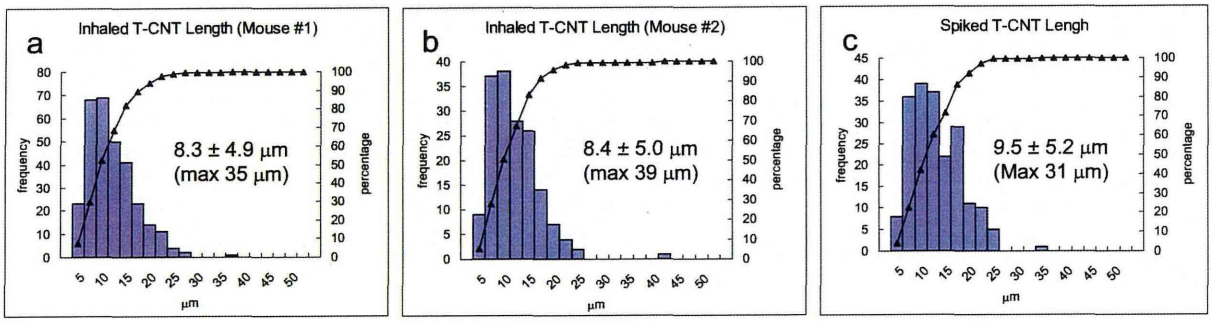


**Fig. 9.** T-CNT recovered from the mouse lung. a, b) Length distribution of T-CNT in the lung of two mice exposed 2 hr a day for 5 days at an average concentration of 1.8 mg/m$^3$ (n = 306 and 166 each, mean ± s.d). c) Length distribution of T-CNT (1 μg) spiked to a non-exposed mouse lung (n = 198, mean ± s.d).


**Fig. 10.** T-CNT recovered from the mouse lung. a) SEM of the sediment of the dissolved lung of a mouse exposed to T-CNT in an inhalation chamber 2 hr a day for 5 days, x 2,000. Long and short single fibers are shown to be inhaled (treated with solution containing EDTA and ascorbic acid). b) SEM of a same sample treated without EDTA and ascorbic. The debris covering the fibers is considered to be iron-based amorphous substances soluble to EDTA, x 2,000. Ascorbic acid was found to be effective in keeping iron ions to be bivalent (ferrous) and soluble. (scale bars are 10 μm)

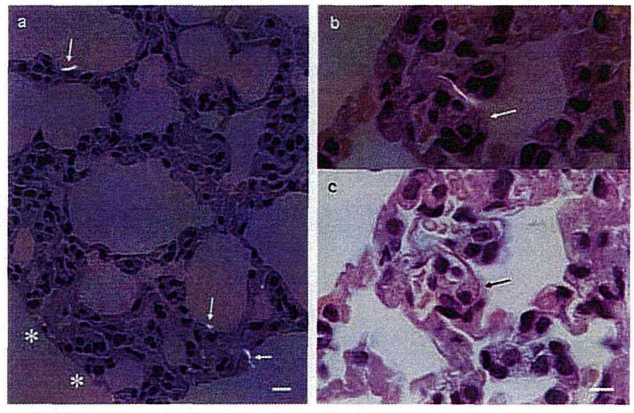


**Fig. 11.** a) A polarized microscopic view of the alveolar region of a lung exposed to 1 mg/m$^3$ of T-CNT for 2 hr a day for 5 days. Arrows indicate single T-CNTs deposited in alveolar spaces phagocytized by alveolar macrophages. Asterisks indicates visceral pleural. (scale bar 10 μm) b,c) Another portion of alveolar region with a tadpole-shaped alveolar macrophage containing single long CNT in its cytoplasm shown in plain and polarized view. The lungs shown here are not inflated with formalin at fixation in order to avoid replacement of the CNTs. (scale bar 5 μm)

without inflammatory or granulomatous response, morphologically interpretable as a view of expectoration by the ciliary movement of the bronchial epithelium. There were no dense aggregates/agglomerates in the lungs so far as examined. In the peripheral alveolar space, single fibers are found phagocytized in alveolar macrophages as shown in Fig. 11. There were only mild inflammatory reactions such as neutrophilic migration against fibers in mucous blanket of the bronchial/bronchiolar segments and fibers in the alveolar space.

## DISCUSSION

The MWCNT treated with the "Taquann" method (T-CNT) consisted of highly dispersed single fibers with marked reduction of aggregates/agglomerates, both in the aerosol and in the resuspended solution. The length and width distribution of the single fibers were not different between the T-CNT and the original U-CNT, indicating that this method is physically mild to the sample and does not shorten the fibers.

The Taquann method consists of two major steps, the

efficient filtration in liquid phase and the idea of critical point drying in order to prevent re-aggregation of the fibers by surface tension during drying. The latter step was inspired by the drying method for SEM samples. TB-sublimation technique used in this study is an alternative method used for SEM samples as well. Our trial-and-error added a few innovations such as gentle kneading of half-frozen TB suspension and a freeze-and-thaw process for a better dispersion (visible differences in fineness of suspension, data not shown), and vibration of the sieve for a faster and better yield of filtrate (approximately 7 fold increase in half the time). This Taquann method does not use high power sonication or other strong mechanical shearing, so that the length distribution of the single fibers did not change. The equipments and reagents used here are mostly available at regular biological or chemical laboratories. The new aerosol generating system by the direct injection of T-CNT had successfully generated highly dispersed aerosol of MWNT-7 and an exposure study confirmed the inhalation of MWNT-7 single fibers in mouse lung down to the peripheral alveolar spaces. In this condition, i.e. five consequtive days of 2 hr exposure, histologically, there were only mild neutrophilic infiltration. A long-term follow up study is underway.

It is highly plausible that the Taquann method can be applied to other types of particles as long as they are not soluble to TB (additional study in preparation). Well-dispersed samples generated by the Taquann method, together with the direct injection and the small scale inhalation chamber system, would facilitate the inhalation toxicity studies more relevant to human exposure not only at the big facilities but also at the small scaled laboratories.

Finally, this dispersion method may also be useful for industries where difficulty in dispersion of nanoparticles was a limiting process in developing new products. For a large scale manufacturing, carbon dioxide critical point drying may be suitable than TB sublimation.

## ACKNOWLEDGMENT

The authors thank Dr. Hiroyuki Tsuda for introducing the metal sieve for liquid phase filtration. This study is supported by the Health Sciences Research Grants H21-kagaku-ippan-008, H23-kagaku-ippan-005 and H24-kagaku-shitei-009 from the Ministry of Health, Labour and Welfare, Japan.

## REFERENCES

Ahn, K.H., Kim, S.M. and Yu, I.J. (2011): Multi-walled carbon nanotube (MWCNT) dispersion and aerosolization with hot water atomization without addition of any surfactant. Saf. Health Work., **2**, 65-69.

Gasser, M., Wick, P., Clift, M.J., Blank, F., Diener, L., Yan, B., Gehr, P., Krug, H.F. and Rothen-Rutishauser, B. (2012): Pulmonary surfactant coating of multi-walled carbon nanotubes (MWCNTs) influences their oxidative and pro-inflammatory potential in vitro. Part Fibre Toxicol., **9**, 17.

Han, J.H., Lee, E.J., Lee, J.H., So, K.P., Lee, Y.H., Bae, G.N., Lee, S.B., Ji, J.H., Cho, M.H. and Yu, I.J. (2008): Monitoring multiwalled carbon nanotube exposure in carbon nanotube research facility. Inhal. Toxicol., **20**, 741-749.

Kasai, T., Gotoh, K., Nishizawa, T., Sasaki, T., Katagiri, T., Umeda, Y., Toya, T. and Fukushima, S. (2013): Development of a new multi-walled carbon nanotube (MWCNT) aerosol generation and exposure system and confirmation of suitability for conducting a single-exposure inhalation study of MWCNT in rats. Nanotoxicology, (in press).

Mercer, R.R., Hubbs, A.F., Scabilloni, J.F., Wang, L., Battelli, L.A., Friend, S., Castranova, V. and Porter, D.W. (2011): Pulmonary fibrotic response to aspiration of multi-walled carbon nanotubes. Part Fibre. Toxicol., **8**, 21.

Mercer, R.R., Scabilloni, J., Wang, L., Kisin, E., Murray, A.R., Schwegler-Berry, D., Shvedova, A.A. and Castranova, V. (2008): Alteration of deposition pattern and pulmonary response as a result of improved dispersion of aspirated single-walled carbon nanotubes in a mouse model. Am. J. Physiol. Lung Cell. Mol. Physiol., **294**, L87-97.

Mitchell, L.A., Gao, J., Wal, R.V., Gigliotti, A., Burchiel, S.W. and McDonald, J.D. (2007): Pulmonary and systemic immune response to inhaled multiwalled carbon nanotubes. Toxicol. Sci., **100**, 203-214.

Morimoto, Y., Hirohashi, M., Ogami, A., Oyabu, T., Myojo, T., Todoroki, M., Yamamoto, M., Hashiba, M., Mizuguchi, Y., Lee, B.W., Kuroda, E., Shimada, M., Wang, W.N., Yamamoto, K., Fujita, K., Endoh, S., Uchida, K., Kobayashi, N., Mizuno, K., Inada, M., Tao, H., Nakazato, T., Nakanishi, J. and Tanaka, I. (2011): Pulmonary toxicity of well-dispersed multi-wall carbon nanotubes following inhalation and intratracheal instillation. Nanotoxicology, **6**, 587-599.

Muller, J., Huaux, F., Moreau, N., Misson, P., Heilier, J.F., Delos, M., Arras, M., Fonseca, A., Nagy, J.B. and Lison, D. (2005): Respiratory toxicity of multi-wall carbon nanotubes. Toxicol. Appl. Pharmacol., **207**, 221-231.

Oyabu, T., Myojo, T., Morimoto, Y., Ogami, A., Hirohashi, M., Yamamoto, M., Todoroki, M., Mizuguchi, Y., Hashiba, M., Lee, B.W., Shimada, M., Wang, W.N., Uchida, K., Endoh, S., Kobayashi, N., Yamamoto, K., Fujita, K., Mizuno, K., Inada, M., Nakazato, T., Nakanishi, J. and Tanaka, I. (2011): Biopersistence of inhaled MWCNT in rat lungs in a 4-week well-characterized exposure. Inhal. Toxicol., **23**, 784-791.

Poland, C.A., Duffin, R., Kinloch, I., Maynard, A., Wallace, W.A., Seaton, A., Stone, V., Brown, S., Macnee, W. and Donaldson, K. (2008): Carbon nanotubes introduced into the abdominal cavity of mice show asbestos-like pathogenicity in a pilot study. Nat Nanotechnol., **3**, 423-428.

Porter, D.W., Hubbs, A.F., Mercer, R.R., Wu, N., Wolfarth, M.G., Sriram, K., Leonard, S., Battelli, L., Schwegler-Berry, D.,

Friend, S., Andrew, M., Chen, B.T., Tsuruoka, S., Endo, M. and Castranova, V. (2009): Mouse pulmonary dose- and time course-responses induced by exposure to multi-walled carbon nanotubes. Toxicology, **269**, 136-147.

Pott, F., Roller, M., Kamino, K. and Bellmann, B. (1994): Significance of durability of mineral fibers for their toxicity and carcinogenic potency in the abdominal cavity of rats in comparison with the low sensitivity of inhalation studies. Environ. Health Perspect., **102 Suppl. 5**, 145-150.

Roller, M., Pott, F., Kamino, K., Althoff, G.H. and Bellmann, B. (1997): Dose-response relationship of fibrous dusts in intraperitoneal studies. Environ. Health Perspect., **105 Suppl. 5**, 1253-1256.

Shvedova, A.A., Kisin, E., Murray, A.R., Johnson, V.J., Gorelik, O., Arepalli, S., Hubbs, A.F., Mercer, R.R., Keohavong, P., Sussman, N., Jin, J., Yin, J., Stone, S., Chen, B.T., Deye, G., Maynard, A., Castranova, V., Baron, P.A. and Kagan, V.E. (2008): Inhalation vs. aspiration of single-walled carbon nanotubes in C57BL/6 mice: inflammation, fibrosis, oxidative stress, and mutagenesis. Am. J. Physiol. Lung Cell. Mol. Physiol., **295**, L552-565.

Takagi, A., Hirose, A., Futakuchi, M., Tsuda, H. and Kanno, J. (2012): Dose-dependent mesothelioma induction by intraperitoneal administration of multi-wall carbon nanotubes in p53 heterozygous mice. Cancer Sci., **103**, 1440-1444.

Takagi, A., Hirose, A., Nishimura, T., Fukumori, N., Ogata, A., Ohashi, N., Kitajima, S. and Kanno, J. (2008): Induction of mesothelioma in p53+/- mouse by intraperitoneal application of multi-wall carbon nanotube. J. Toxicol. Sci., **33**, 105-116.

Wang, X., Katwa, P., Podila, R., Chen, P., Ke, P.C., Rao, A.M., Walters, D.M., Wingard, C.J. and Brown, J.M. (2011): Multi-walled carbon nanotube instillation impairs pulmonary function in C57BL/6 mice. Part Fibre. Toxicol., **8**, 24.

Wang, X., Xia, T., Duch, M.C., Ji, Z., Zhang, H., Li, R., Sun, B., Lin, S., Meng, H., Liao, Y.P., Wang, M., Song, T.B., Yang, Y., Hersam, M.C. and Nel, A.E. (2012): Pluronic F108 coating decreases the lung fibrosis potential of multiwall carbon nanotubes by reducing lysosomal injury. Nano Lett., **12**, 3050-3061.

Warheit, D.B., Laurence, B.R., Reed, K.L., Roach, D.H., Reynolds, G.A. and Webb, T.R. (2004): Comparative pulmonary toxicity assessment of single-wall carbon nanotubes in rats. Toxicol. Sci., **77**, 117-125.

Xu, J., Futakuchi, M., Shimizu, H., Alexander, D.B., Yanagihara, K., Fukamachi, K., Suzui, M., Kanno, J., Hirose, A., Ogata, A., Sakamoto, Y., Nakae, D., Omori, T. and Tsuda, H. (2012): Multi-walled carbon nanotubes translocate into the pleural cavity and induce visceral mesothelial proliferation in rats. Cancer Sci., **103**, 2045-2050.

1521-0103/347/1/145–153$25.00
THE JOURNAL OF PHARMACOLOGY AND EXPERIMENTAL THERAPEUTICS

http://dx.doi.org/10.1124/jpet.113.205138
J Pharmacol Exp Ther 347:145–153, October 2013

# Enhancement of $Ca^{2+}$ Influx and Ciliary Beating by Membrane Hyperpolarization due to ATP-Sensitive $K^+$ Channel Opening in Mouse Airway Epithelial Cells

Teruya Ohba, Eiji Sawada, Yoshiaki Suzuki, Hisao Yamamura, Susumu Ohya, Hiroyuki Tsuda, and Yuji Imaizumi

*Department of Molecular and Cellular Pharmacology, Graduate School of Pharmaceutical Sciences (T.O., E.S., Y.S., H.Y., Y.I.) and Nanomaterial Toxicology Project (H.T.), Nagoya City University, Nagoya, Japan; and Department of Pharmacology, Division of Pathological Sciences, Kyoto Pharmaceutical University, Kyoto, Japan (S.O.)*

Received March 25, 2013; accepted August 5, 2013

**ABSTRACT**

Among the several types of cells composing the airway epithelium, the ciliary cells are responsible for one of the most important defense mechanisms of the airway epithelium: the transport of inhaled particles back up into the throat by coordinated ciliary movement. Changes in the cytoplasmic $Ca^{2+}$ concentration ($[Ca^{2+}]_i$) are the main driving force controlling the ciliary activity. In mouse ciliary cells, membrane hyperpolarization from −20 to −60 mV under whole-cell voltage-clamp induced a slow but significant $[Ca^{2+}]_i$ rise in a reversible manner. This rise was completely inhibited by the removal of $Ca^{2+}$ from the extracellular solution. Application of diazoxide, an ATP-dependent $K^+$ channel opener, dose-dependently induced a membrane hyperpolarization ($EC_{50}$ = 2.3 μM), which was prevented by the addition of 5 μM glibenclamide. An inwardly rectifying current was elicited by the application of 10 μM diazoxide and suppressed by subsequent addition of 5 μM glibenclamide. Moreover, the application of 10 μM diazoxide induced a significant $[Ca^{2+}]_i$ rise and facilitated ciliary movement. Multi-cell reverse-transcription polymerase chain reaction analyses and immunocytochemical staining suggested that the subunit combination of Kir6.2/SUR2B and possibly also Kir6.1/SUR2B is expressed in ciliary cells. The confocal $Ca^{2+}$ imaging analyses suggested that the $[Ca^{2+}]_i$ rise induced by diazoxide occurred preferentially in the apical submembrane region. In conclusion, the application of a $K_{ATP}$ channel opener to airway ciliary cells induces membrane hyperpolarization and thereby induces a $[Ca^{2+}]_i$ rise via the facilitation of $Ca^{2+}$ influx through the non–voltage-dependent $Ca^{2+}$ permeable channels. Therefore, a $K_{ATP}$ opener may be beneficial in facilitating ciliary movement.

## Introduction

The regulation of $K^+$ channel conductance is suggested to be a critical issue in the therapy of asthma and/or chronic obstructive pulmonary disease (Pelaia et al., 2002; Malerba et al., 2010). The activation of the ATP-sensitive $K^+$ ($K_{ATP}$) channel, the large conductance $Ca^{2+}$-activated $K^+$ (BK) channel, or the intermediate conductance $Ca^{2+}$-activated $K^+$ (IK) channel by specific modulators induces the following: bronchodilation, reduced airway hyperresponsiveness, reduced mucus production and cough, suppressed airway inflammation, and the remodeling of the preclinical models of asthma and chronic obstructive pulmonary disease (Malerba et al., 2010).

Ciliary cells play a fundamental role in the airway self-defense system by removing foreign materials from the airways in functional combinations with the other types of epithelial cells. The motile cilia in the airway epithelium are the engines for mucociliary clearance, which is a mechanism responsible for cleaning the airways of inhaled particles. The ciliary beating observed in the human airway epithelium is principally due to a slow constitutive rate of beating caused by inherent and spontaneous dynein ATPase activity. The cilia can increase their beating frequency by the activation of several different control mechanisms, one of these being changes in the intracellular $Ca^{2+}$ concentration ($[Ca^{2+}]_i$) (Evans and Sanderson, 1999; Schmid and Salathe, 2011). Aside from the regulatory effects of calcium on the ciliary beating rate, calcium is also involved in the complex task of synchronizing the beat among the cilia of one single cell as well as between the cilia on multiple cells (Schmid and Salathe, 2011).

This investigation was supported by a Grant-in-Aid for Scientific Research on Priority Areas [Grant 23136512] (to Y.I.) from the Ministry of Education, Culture, Sports, Science, and Technology in Japan; and by a Grant-in-Aid for Scientific Research [Grant 23390020] (to Y.I.) from the Japan Society for the Promotion of Science. This work was also supported by Health and Labor Sciences Research grants from the Ministry of Health, Labor and Welfare, Japan [Research on Risk of Chemical Substance 21340601, H19-kagaku-ippan-006, and H22-kagaku-ippan-005] (to H.T.).
T.O. and E.S. contributed equally to this study.
dx.doi.org/10.1124/jpet.113.205138

**ABBREVIATIONS:** BK, large conductance $Ca^{2+}$-activated $K^+$ channel; $[Ca^{2+}]_i$, intracellular $Ca^{2+}$ concentration; CBF, ciliary beating frequency; DPBS, Dulbecco's phosphate-buffered saline; fluo-4/AM, fluo-4 acetoxymethyl ester; fura-2/AM, fura-2 acetoxymethyl ester; $K_{ATP}$ channel, ATP-sensitive $K^+$ channel; NGS, normal goat serum; PBS, phosphate-buffered saline; PCR, polymerase chain reaction; SUR, sulfonylurea receptor; VDCC, voltage-dependent $Ca^{2+}$ channel.

Initially, $K_{ATP}$ channels were identified as the key molecules for insulin secretion in pancreatic $\beta$-cells; they are now well known to be ubiquitously expressed in a variety of tissues as the molecular combination of channel-forming Kir6.x subunits and sulfonylurea receptors (SURs) (Clark and Proks, 2010; Flagg et al., 2010; Hibino et al., 2010). Although the expression of $K_{ATP}$ channels has been reported in alveolar cells (Trinh et al., 2007) and cell lines derived from human airway epithelial tissues (Trinh et al., 2008), their functional expression in ciliary cells has not yet been documented. Previous studies have revealed that ATP and acetylcholine are major endogenous stimulants that facilitate ciliary beating by activating the purinoceptors and by increasing $[Ca^{2+}]_i$, which, in turn, may induce membrane hyperpolarization via the activation of $Ca^{2+}$-dependent $K^+$ channels (Weiss et al., 1992; Tarasiuk et al., 1995). However, conflicting reports have been published on whether changes in the membrane potential can significantly affect the ciliary beat frequency (Ma et al., 2002). Therefore, the present study was undertaken to elucidate the effects of $K_{ATP}$ openers on ciliary beating rates and to determine the underlying mechanisms of the changes. The effects of $K_{ATP}$ openers on ciliary beating may be a key issue in evaluating their therapeutic potentials for respiratory diseases.

## Materials and Methods

**Animals.** C57BL/6N male mice (Japan SLC, Hamamatsu, Japan), 8 to 12 weeks old, were used. All experiments were carried out in accordance with the Guiding Principles for the Care and Use of Laboratory Animals of the Japanese Pharmacological Society and also with the approval of the Ethics Committee of Nagoya City University.

**Isolation of Single Ciliary Cells.** The tracheas were removed from the mice. The epithelium was separated from the cartilage and cut into squares of approximately 1 × 1 mm. The tissue was maintained in Dulbecco's phosphate-buffered saline (DPBS) containing (in mM): 137 NaCl, 2.7 KCl, 0.9 $CaCl_2$, 0.5 $MgCl_2$, 8 $Na_2HPO_4$, 1.47 $KH_2PO_4$, and 5 glucose, pH 7.4. The epithelium was incubated for 25 minutes at 37°C in DPBS supplemented with 13 U/ml papain (Sigma-Aldrich, St. Louis, MO), 1 mg/ml bovine serum albumin (Sigma-Aldrich), and 1 mg/ml 1,4-dithiothreitol (Wako Pure Chemicals, Osaka, Japan). After incubation, the solution was replaced with DPBS. The cells were then dispersed several times with a fire-polished Pasteur pipette. The isolated cells were immediately used following the cell dispersion. All of the experiments were carried out at room temperature (25°C).

**Multicell Reverse-Transcription Polymerase Chain Reaction.** Approximately 40 ciliary cells were collected by the glass electrode of ~2-30 $\mu$m in diameter. Total RNA was extracted from them using NucleoSpin RNA XS (Macherey Nagel, Düren, Germany) and reverse-transcribed using oligo$(dT)_{12-18}$ primer and SuperScript II reverse transcriptase (Invitrogen, Carlsbad, CA). The solution without RTase was used as a negative control. The polymerase chain reaction (PCR) amplification profile using KOD-Plus-Neo (TOYOBO, Tokyo, Japan) and GeneAmp PCR System 2700 (Applied Biosystems, Foster City, CA) was as follows: a 10-second denaturation step at 98°C, a 30-second annealing step at 55°C, and a 60-second primer extension step at 72°C for 35 cycles. Gene products were analyzed by 2.0% agarose gel electrophoresis.

**PCR Primers.** The following PCR primers were used: for mouse Kir6.1/Kcnj8 (GenBank Accession No. NM_008428), (+) 5′-CAA GTG ACC ATT GGG TTT GGA-3′ and (−) 5′-CGT TGA TGA TCA GAC CCA CGA-3′ (100 bp); Kir6.2/Kcnj11 (NM_010602), (+) 5′-CAA GAA AGG CAA CTG CAA CGT-3′ and (−) 5′-TGT GTG GCC ATT TGA GGT CCA-3′ (101 bp); SUR1/Abcc8 (NM_011510), (+) 5′-AGT GAA GCC CCC TGA GGA CCT-3′ and (−) 5′-GAT GAA GGC ATT CAT CCA CCA-3′ (103 bp); SUR2/Abcc9 (NM_021041 and NM_011511), (+) 5′-TAC GAA CAT CAT CGA CCA GCA-3′ and (−) 5′-AAA CAC GGG TGT AGC ATA GGA-3′ (109 bp); $\beta$-actin/Actb (NM_007393), 5′-AGG CCA ACC GTG AAA AGA TG-3′ and (−) 5′-ACC AGA GGC ATA CAG GGA CA-3′ (101 bp). The specific primers for the spliced variant analysis of SUR2 were designed as follows: for mouse SUR2A/Abcc9A (NM_021041), (+) 5′-TCT TCT ATT GTG GAT GCA GGC CT-3′ and (−) 5′-CTA CTT GTT GGT CAT CAC CAA AGT-3′ (129 bp); SUR2B/Abcc9B (NM_011511), (+) 5′-CAC ACC ATT CTG ACT GCA GAC CT-3′ and (−) 5′-TCA CAT GTC TGC ACG GAC AAA CGA-3′ (129 bp).

**Immunocytochemistry.** Polyclonal antimouse Kir6.2 (APC-020) and control antigen were purchased from Alomone Laboratories (Jerusalem, Israel). Polyclonal antibodies to Kir6.1 (R-14), SUR1 (H-80), SUR2A (M-19), SUR2B (C-15) and each blocking peptide were purchased from Santa Cruz Biotechnology, Inc. (Dallas, TX). Dissociated ciliary cells were settled down on coverslips precoated with poly-L-lysine (Matsunami Glass Industry, Osaka, Japan). These cells were fixed with 4% paraformaldehyde for 20 minutes and permeabilized with 0.2% Triton/phosphate-buffered saline (PBS) for 15 minutes at room temperature. After rinsing in PBS containing 1% normal goat serum (NGS), the cells were preincubated for 1 hour with 10% NGS/PBS to minimize nonspecific binding of antibodie, and incubated successively with 1:100 diluted antibodies for 12 hours. Primary antibodies were extensively washed with 1% NGS/PBS and incubated with Alexa 488-conjugated antirabbit IgG goat or Alexa 488-conjugated antigoat IgG rabbit antiserum (Molecular Probe, Eugene, OR) for 1 hour. Immunostained cells were observed using an A1R laser-scanning confocal fluorescent microscope (Nikon, Tokyo, Japan) equipped with a fluorescent microscope (ECLIPSE Ti; Nikon), an objective lens (Plan Apo 60× 1.40 NA oil immersion; Nikon), and NIS Elements software (version 3.10; Nikon). The excitation wavelength from the multiargon laser (Melles Griot, Carlsbad, CA) for Alexa 488 was 488 nm, and the emission light was collected by a band-pass filter (525/50 nm).

**Electrophysiological Recordings.** A whole-cell patch clamp was applied to a single ciliary cell with a patch pipette using a CEZ-2400 amplifier (Nihon Kohden, Tokyo, Japan) as previously described (Imaizumi et al., 1989; Yamamura et al., 2012). The membrane currents and voltage signals were stored and analyzed using a Digidata 1440A and a pCLAMP 10.2 (Axon Instruments, Foster City, CA). The ciliary cells were clamped at a holding potential of −40 mV, and a descending ramp protocol from +40 to −120 mV for 500 milliseconds was performed every 10 seconds. In some experiments, membrane potentials from single ciliary cells were measured under the current-clamp mode in whole-cell configuration.

**Measurement of the $Ca^{2+}$ Fluorescence Ratio and the $Ca^{2+}$ Images.** The airway ciliary cells were loaded with 10 $\mu$M fura-2 acetoxymethyl ester (fura-2/AM; Molecular Probes) in a standard HEPES solution for 45 minutes at room temperature. The fura-2 fluorescent signals were measured using the Argus/HiSCA imaging system (Hamamatsu Photonics, Hamamatsu, Japan). In some experiments, in which simultaneous measurements of $[Ca^{2+}]_i$ and membrane potential were taken, ciliary cells were loaded with 100 $\mu$M fluo-4 (Molecular Probes) by diffusion from the recording pipette (Funabashi et al., 2010). The $Ca^{2+}$ images were scanned every 2 seconds.

**Intracellular $Ca^{2+}$ Images by Use of Fluo-4/AM and Confocal Fluorescent Microscopy.** The airway ciliary cells were loaded with 10 $\mu$M fluo-4 acetoxymethyl ester (fluo-4/AM; Molecular Probes) in a standard HEPES solution for 45 minutes at room temperature. The cytosolic $Ca^{2+}$ images were obtained using the aforementioned laser-scanning confocal fluorescent microscope and NIS Elements software. The excitation wavelength for fluo-4 was 488 nm, and the emission wavelength was collected by a bandpass filter (525/50 nm). The resolution of the microscope was 0.414 $\mu$m per pixel and 2.02 $\mu$m to the *Z*-axis direction. The confocal images were scanned over a full frame (512 × 512 pixels) every 2 seconds.

**Membrane Potential Measurements by Voltage-Sensitive Fluorescent Dye.** The membrane potential was measured as previously reported (Yamazaki et al., 2011) using 100 nM $DiBAC_4(3)$ (Dojin,

Kumamoto, Japan), a bis-barbituric acid oxonol dye with an excitation maximum at approximately 488 nm. The data were collected and analyzed using the Argus/HiSCA imaging system. The sampling interval of the $DiBAC_4(3)$ fluorescence measurements was every 5 seconds.

**Measurement of Ciliary Beating Frequency.** The ciliary beating frequency (CBF) of the tracheal airway ciliary cell (Shiima-Kinoshita et al., 2004; Kawakami et al., 2004) was measured at 100 Hz using a high-speed resolution CCD camera (C9100-12, Hamamatsu Photonics). Prior to the experiments, the CBFs were measured every 1 minute for 2 minutes, and the average value of these three CBFs were used as the basal CBF ($CBF_0$) in the HEPES-buffered solution. Any changes in the CBF were expressed as a CBF ratio.

**Solutions.** An extracellular solution was made using a standard HEPES-buffered solution composed of the following (in mM): 137 NaCl, 5.9 KCl, 2.2 $CaCl_2$, 1.2 $MgCl_2$, 14 glucose, and 10 HEPES. The pH of the solution was adjusted with NaOH to 7.4. The $K_{ATP}$ current was measured in a 40 mM $K^+$ HEPES-buffered solution composed of the following (in mM): 99.7 NaCl, 40 KCl, 2.2 $CaCl_2$, 1.2 $MgCl_2$, 14 glucose, and 10 HEPES. The pH of the solution was adjusted with NaOH to 7.4. The pipette solution for electrical recordings contained the following (in mM): 140 KCl, 4 $MgCl_2$, 2 ATP-$Na_2$, 0.05 EGTA, 10 HEPES. The pH of the solution was adjusted with KOH to 7.2. All experiments were undertaken at room temperature to avoid fura-2 trapping in organelles and dye leakage at 37°C.

**Statistical Analysis.** The pooled data are expressed as means ± S.E., and the statistical significance was examined using Student's $t$ test for two groups and Tukey's for three or more groups. $P$ values < 0.05 were considered statistically significant. The data of the relationship between diazoxide and fluorescent signal were fitted using the following equation after normalization: $F/F_0 = 1 - (1 - C)/\{1 + (K_d/[\text{diazoxide}])^n\}$, where $C$ is the component resistant, $K_d$ is the apparent dissociation constant, [diazoxide] is the concentration, and $n$ is the Hill coefficient (Fig. 2D).

**Drugs.** The pharmacological reagents were obtained from Sigma-Aldrich. Diazoxide, glibenclamide, and pinacidil were dissolved in dimethylsulfoxide at concentrations of 5 to 10 mM as a stock solution.

## Results

**The Effects of $K_{ATP}$ Opener on Ciliary Beating.** The ciliary movement in freshly isolated mice ciliary cells was recorded at 100 Hz using a high time-resolution video camera and analyzed using a slow image reproduction (Fig. 1A). The application of 10 $\mu$M diazoxide, a $K_{ATP}$ channel opener, significantly increased the frequency of the ciliary movement (Fig. 1B), and the effect lasted for over 10 minutes (not shown). The addition of 5 $\mu$M glibenclamide, a $K_{ATP}$ channel blocker, removed the diazoxide-induced enhancement of the frequency (Fig. 1B). The summarized data (Fig. 1C) indicate a significant enhancement of the frequency when 10 $\mu$M diazoxide was applied ($n = 6$, $P < 0.05$ versus control) and a significant inhibition of the frequency when 5 $\mu$M glibenclamide was added ($n = 6$, $P < 0.01$ versus diazoxide alone). Although the amplitude of the movement may also be increased by the diazoxide, those quantitative analyses could not be done during this study due to the limited time resolution of the video system.

**The $K_{ATP}$ Opener–Induced Membrane Hyperpolarization and the Subsequent Rise in $[Ca^{2+}]_i$.** The membrane potential changes induced by the addition of 10 $\mu$M diazoxide in the isolated ciliary cells were measured using the voltage sensitive fluorescent dye $DiBAC_4(3)$.

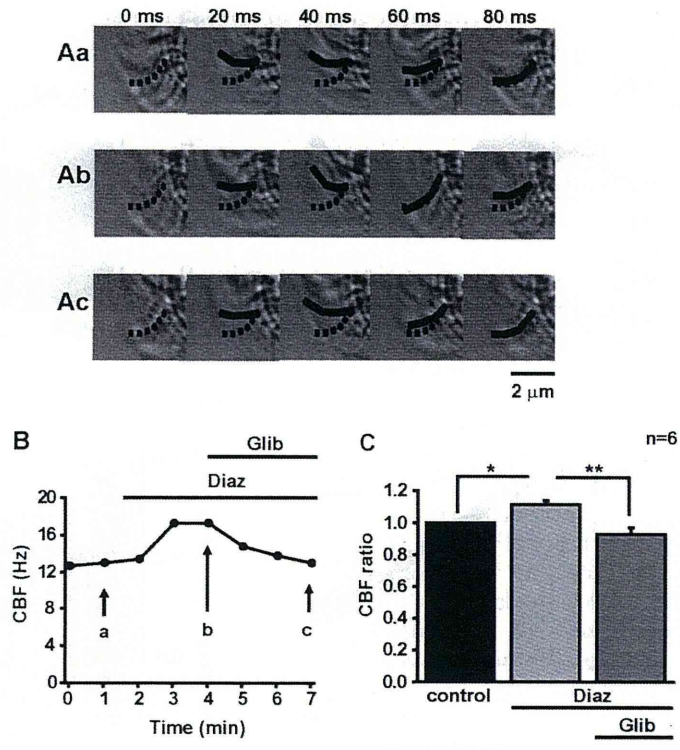


**Fig. 1.** The enhancement of the ciliary movement by diazoxide. (A) The ciliary movement in an epithelial cell isolated from a mouse trachea was recorded with a high-speed digital camera at 100 Hz. The CBF was directly measured from the images as shown by the dotted and solid lines. The series of images (a, b, and c) were obtained at the time shown in B. (B) The time course of CBF in HEPES-buffered solution, in the presence of 10 $\mu$M diazoxide (Diaz), and following the addition of 5 $\mu$M glibenclamide (Glib). (C) The summarized data concerning the effects of diazoxide and glibenclamide ($n = 6$). *,**$P < 0.05$ and 0.01, respectively.

The sustained decrease in the fluorescence intensity observed following the addition of 10 $\mu$M diazoxide is indicative of membrane hyperpolarization ($n = 5$, $P < 0.01$). The diazoxide-induced decrease in fluorescence intensity was completely removed by the addition of 5 $\mu$M glibenclamide ($n = 5$, $P < 0.01$; Fig. 2, A and B). The diazoxide-induced decrease in fluorescence intensity was concentration-dependent in the range of 1 and 30 $\mu$M (Fig. 2, C and D). The $EC_{50}$ value for membrane potential of the cells treated with diazoxide was 2.3 $\mu$M, and the Hill coefficient was 3.4 ($n = 11$).

The membrane potential was also measured under current-clamp mode in freshly isolated single ciliary cells using pipette filling solution containing 140 mM KCl (see *Materials and Methods*). In all four experiments, stable recordings for over 10 minutes were successfully obtained throughout the procedure of adding two drugs sequentially; the addition of 10 $\mu$M diazoxide induced sustained membrane hyperpolarization of 3.6 ± 1.4 mV from the resting membrane potential of −18.6 ± 1.4 mV ($n = 4$). Further addition of 5 $\mu$M glibenclamide resulted in depolarization by 2.4 ± 0.5 mV ($n = 4$). Taking the initial resting membrane potential in each cell as 1.0, the potentials after the addition of diazoxide and glibenclamide were 1.20 ± 0.03 ($P < 0.01$ versus 1.0) and 1.07 ± 0.03 ($P < 0.05$ versus diazoxide alone).

The effects of the diazoxide on $[Ca^{2+}]_i$ were examined in isolated ciliary cells using fura-2/AM (Fig. 3). The application of 10 $\mu$M diazoxide increased the fluorescence ratio (F340/F380), indicating the increase in $[Ca^{2+}]_i$ ($n = 8$, $P < 0.01$). This

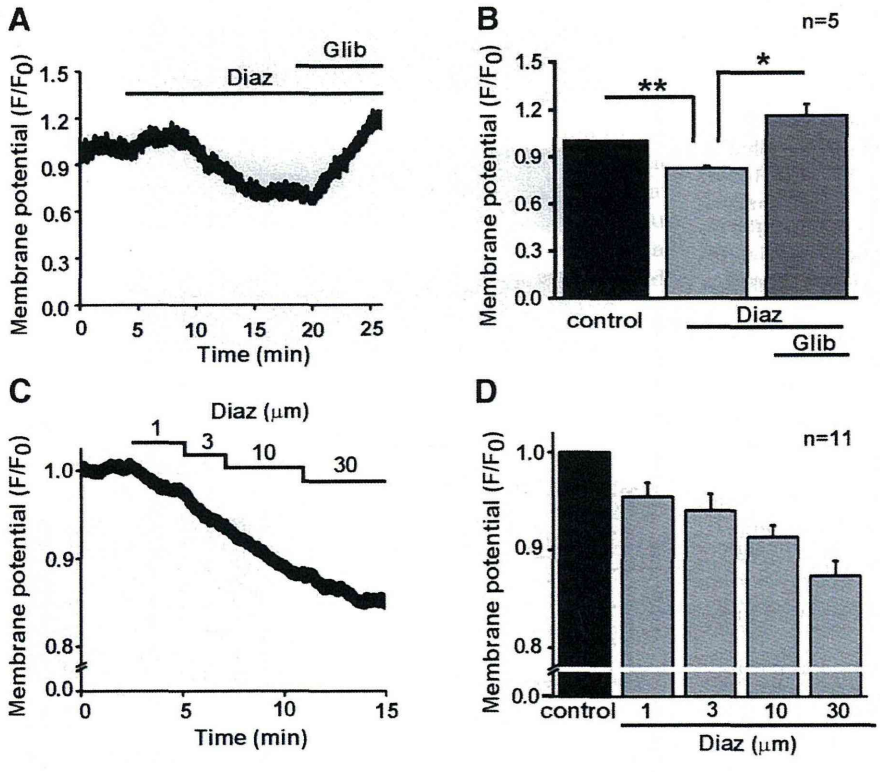


**Fig. 2.** The diazoxide-induced hyperpolarization of the membrane. (A) The changes in the membrane potential were monitored by the voltage-sensitive dye $DiBAC_4(3)$. The changes in the fluorescent intensity ratio ($F/F_0$) that were induced by the addition of 10 $\mu$M diazoxide (Diaz) and 5 $\mu$M glibenclamide (Glib) were plotted against time. The average fluorescent intensity ($F$) measured immediately prior to the application of the diazoxide was taken as $F_0$. (B) The summarized data concerning $F/F_0$ are shown ($n$ = 5). *,**$P < 0.05$ and 0.01, respectively. (C) The changes in $F/F_0$ that were induced by the cumulative additions of diazoxide in a dose range from 1 to 30 $\mu$M were plotted against time. (D) The summarized data concerning $F/F_0$ are shown ($n$ = 11). The $EC_{50}$ value and Hill coefficient were 2.3 and 3.4 $\mu$M, respectively.

observed increase was removed by the addition of 5 $\mu$M glibenclamide ($n$ = 8, $P < 0.01$). The $[Ca^{2+}]_i$ was also increased by the application of 10 $\mu$M pinacidil, another $K_{ATP}$ channel opener ($n$ = 5, $P < 0.01$), and the effect was again reversed by the addition of 5 $\mu$M glibenclamide ($n$ = 5, $P <$ 0.01).

**The Expression of ATP-Sensitive $K^+$ Channels in Ciliary Cells.** The molecular characteristics of the $K_{ATP}$ channels in the ciliary cells were examined by multicell reverse-transcription PCR analysis. These analyses reveal that the transcripts of Kir6.2 and SUR2B were predominantly expressed in the ciliary cells ($n$ = 3; Fig. 4A).

To clarify protein expression of these channels, immunocytochemical analyses were performed ($n$ = 3; Fig. 4B). Kir6.1, Kir6.2 and SUR2B proteins were detected on plasma membrane of ciliary cells. However, SUR2A did not show significant membrane surface expression. These results are consistent with those from reverse-transcription PCR analyses and strongly suggest that Kir6.2/SUR2B and possibly also Kir6.1/SUR2B are predominantly expressed in mouse ciliary cells. We did not expect to find that SUR1 showed specific expression on cilia.

**The Measurement of ATP-Sensitive $K^+$ Channel Currents in Ciliary Cells.** The $K_{ATP}$ channel current was measured in a single ciliary cell using a whole-cell patch-clamp recording. To amplify the conductance of the Kir channel, the recordings were performed in an external solution containing 40 mM $K^+$. The current–voltage relationship in the control showed slight inward rectification at potentials negative to −60 mV. The inwardly rectifying current was markedly enhanced by the application of 10 $\mu$M diazoxide (Fig. 5A). The enhanced current was reduced by the addition of 5 $\mu$M glibenclamide. The reversal potential of the current component reduced by glibenclamide in the presence of diazoxide was −33 mV, which is close to the equilibrium potential of $K^+$ under the conditions ($E_K$ = −32 mV). The summarized data (Fig. 5B) clearly indicate that the inward $K^+$ current density at −110 mV was significantly enhanced by the application of diazoxide ($n$ = 7, $P < 0.05$ versus control) and markedly reduced by the addition of glibenclamide ($n$ = 5; $P < 0.05$ versus diazoxide alone).

**The Relationship between the Membrane Potential and $[Ca^{2+}]_i$ in the Isolated Ciliary Cells.** The relationship between the membrane potential and $[Ca^{2+}]_i$ was determined in isolated ciliary cells under a whole-cell voltage-clamp. The single ciliary cells were loaded with fluo-4 from recording pipettes. A membrane hyperpolarization from −20 to −60 mV induced a slow increase in $[Ca^{2+}]_i$ ($n$ = 4, $P < 0.01$) and the return of the potential to −20 mV removed the increase in $[Ca^{2+}]_i$ completely but at a much slower rate ($n$ = 4, $P < 0.05$; Fig. 6, A and B). The $[Ca^{2+}]_i$ increase induced by hyperpolarization was also abolished by the withdrawal of 2.2 mM $Ca^{2+}$ in the external solution ($n$ = 3, $P < 0.01$; Fig. 6, C and D). As shown in Fig. 6, the time courses of $[Ca^{2+}]_i$ elevation varied widely from cell to cell, presumably due to the diversity of cell activities after isolation and also the difference in the load of $Ca^{2+}$ indicator among cells. The summarized data indicate that the $[Ca^{2+}]_i$ increase induced by hyperpolarization from −20 to −60 mV was significant, reversible, and susceptible to external $Ca^{2+}$.

**The Image Analyses of Local $[Ca^{2+}]_i$ Changes by Diazoxide in the Ciliary Cells.** The image analyses of changes in the local $[Ca^{2+}]_i$ were performed using fluo-4/AM and a confocal fluorescent microscope. The changes in the fluorescent intensity of the three areas in the ciliated cell (central, apical, and basolateral areas indicated by "a," "b," and "c," respectively, in Fig. 7A) by the application of 10 $\mu$M

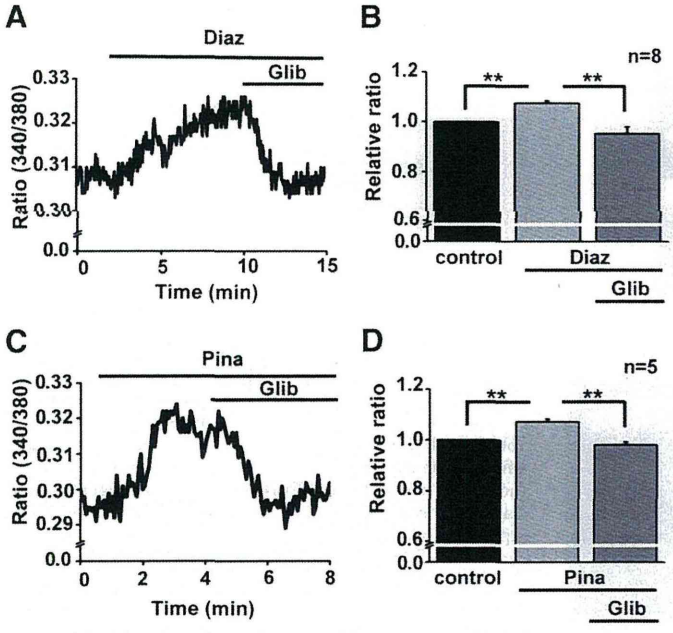


**Fig. 3.** The effects of diazoxide and glibenclamide on $[Ca^{2+}]_i$ in ciliated cells. (A) $[Ca^{2+}]_i$ was measured as fluorescent intensity ratio (*340/380*) in a ciliated cell that was loaded with fura-2/AM. The changes in the ratio induced by the addition of 10 $\mu$M diazoxide (Diaz) and 5 $\mu$M glibenclamide (Glib) were plotted against time. (B) The summarized data concerning the changes in $F/F_0$ are shown ($n$ = 8). The averaged ratio immediately prior to the application of diazoxide was taken as 1.0. $^{**}P < 0.01$. (C) The changes in the ratio induced by the addition of 10 $\mu$M pinacidil (Pina) and 5 $\mu$M glibenclamide (Glib) were plotted against time. (D) The summarized data concerning the changes in $F/F_0$ are shown ($n$ = 5). The averaged ratio immediately prior to the application of the pinacidil was taken as 1.0. $^{**}P < 0.01$.

diazoxide over time were illustrated in Fig. 7B. When the intensity at resting conditions in the cell center was taken as unity, the intensities at the apical area and the basolateral area were 1.01 ± 0.01 and 1.00 ± 0.02, respectively ($n = 9, P >$ 0.05 among the three areas). After the application of 10 $\mu$M diazoxide, the intensities in each area gradually increased (Fig. 7, A and B). The rise in intensity at the apical area was more focal, faster, and larger than the rise in intensity at either the cell center or the basolateral area (Fig. 7C). The summarized data (Fig. 7D) indicate that the rise in intensity at the cell center was significantly less than the rise in intensity at the apical area ($n = 9, P < 0.05$). The rise in intensity at the basolateral area tended to be smaller than the rise in intensity at the apical area, but the difference was not significant.

In addition to the focal rise in submembrane area of the apical side (Fig. 7C, ii and iii), $Ca^{2+}$ rise in the cytosol compartments located deep inside the cell was occasionally observed (Fig. 7C, iii, iv, and v). This type of $Ca^{2+}$ rise was characteristic of a slow rise, deep-inside location, and nonfocal or diffused images. This specific rise was observed to varying degrees in seven of nine cells, whereas the focal and rapid $Ca^{2+}$ rises in the apical submembrane areas were clearly detected in all nine cells examined.

## Discussion

**$Ca^{2+}$ as One of the Major Factors Modulating Mucociliary Motility.** In the ciliary mechanism, the basic mechanism that is responsible for the slow and constitutive rate of beating is considered to be the inherent and spontaneous dynein ATPase activity that depends mainly upon the cellular MgATP concentration (Salathe and Bookman, 1999; Ma et al., 2002). In addition, adapting to the heavier duty of particle transportation with mucus in the epithelium, the upregulation of the ciliary motility by three separate second messengers have been clarified: $Ca^{2+}$, c-AMP, and c-GMP (Salathe, 2007). The cross-talk among signal pathways by these three second messengers has been also revealed. Among these second messengers, $Ca^{2+}$ has fundamental roles in facilitating CBF (Schmid and Salathe, 2011). The application of a $K_{ATP}$ opener increases the CBF by only 10–15% above the baseline in airway ciliated cells. It has been demonstrated, however, that a 16% increase in CBF results in 56% increase in the mucociliary transport velocity in an isolated trachea (Seybold et al., 1990). In this study, the maximum response to the externally applied physiologic stimulants ATP or acetylcholine often resulted in larger rises in $[Ca^{2+}]_i$ than those induced by $K_{ATP}$ openers. These slightly larger increases in CBF (15–30%) suggest that mucociliary clearance may therefore be substantially enhanced by $K_{ATP}$ channel openers.

**New Insight into $[Ca^{2+}]_i$ Regulation by the Membrane Potential Changes in Airway Ciliated Cells.** Information concerning the influence of changes in the membrane potential on the ciliary axoneme movement is not well accumulated and still somewhat controversial. It has been reported that the application of ATP induces a $[Ca^{2+}]_i$ rise, leading to membrane hyperpolarization and facilitates the ciliary motility in frog palate and esophagus ciliated cells (Tarasiuk et al., 1995). In contrast, it has been reported that the membrane potential changes under the whole-cell voltage clamp mode does not induce a significant change in the single-airway ciliated cells of the rabbit (Ma et al., 2002). The findings in the present study clearly demonstrated that the membrane hyperpolarization achieved under a voltage clamp or induced by $K_{ATP}$ channel openers elicited $[Ca^{2+}]_i$ rise and resulted in enhanced ciliary axoneme motility in the airway ciliated cells of the mice. The reason for the discrepancy between the studies in rabbit airway ciliated cells (Ma et al., 2002) and our results in mice is not completely clear. The changes in $[Ca^{2+}]_i$ by membrane hyperpolarization under whole-cell voltage-clamp were not recorded in the former study, presumably because the $[Ca^{2+}]_i$ was fixed by $Ca^{2+}$-EGTA buffer from the pipette filling solution (Ma et al., 2002). In the present study, the pipette solution contained only 50 $\mu$M EGTA and no $CaCl_2$, and the $[Ca^{2+}]_i$ rise by hyperpolarization was consistent and reversible. It is a rather common observation that prolonged membrane hyperpolarization induces a slow but sustained $[Ca^{2+}]_i$ rise in nonexcitable cells, such as T cells, chondrocytes (Funabashi et al., 2010), and vascular endothelial cells (Yamazaki et al., 2011) where the $Ca^{2+}$ permeable channels are functionally expressed but the voltage-gated $Ca^{2+}$ channels are not.

This study differs from the previous, conflicting study (Ma et al., 2002) based on the ATP concentrations used for experimentation. The previous study was conducted using 5 mM MgATP + 0.5 mM $K_2ATP$, whereas the current study was conducted using 4 mM $MgCl_2$ + 2 mM $Na_2ATP$. Although the basic CBF of inherent and spontaneous beating is considered to be dependent on MgATPase activity, the actual MgATP and ATP concentrations in the airway ciliated cells are unknown. It may be possible that experimental conditions in the present study influenced the CBF increase that were

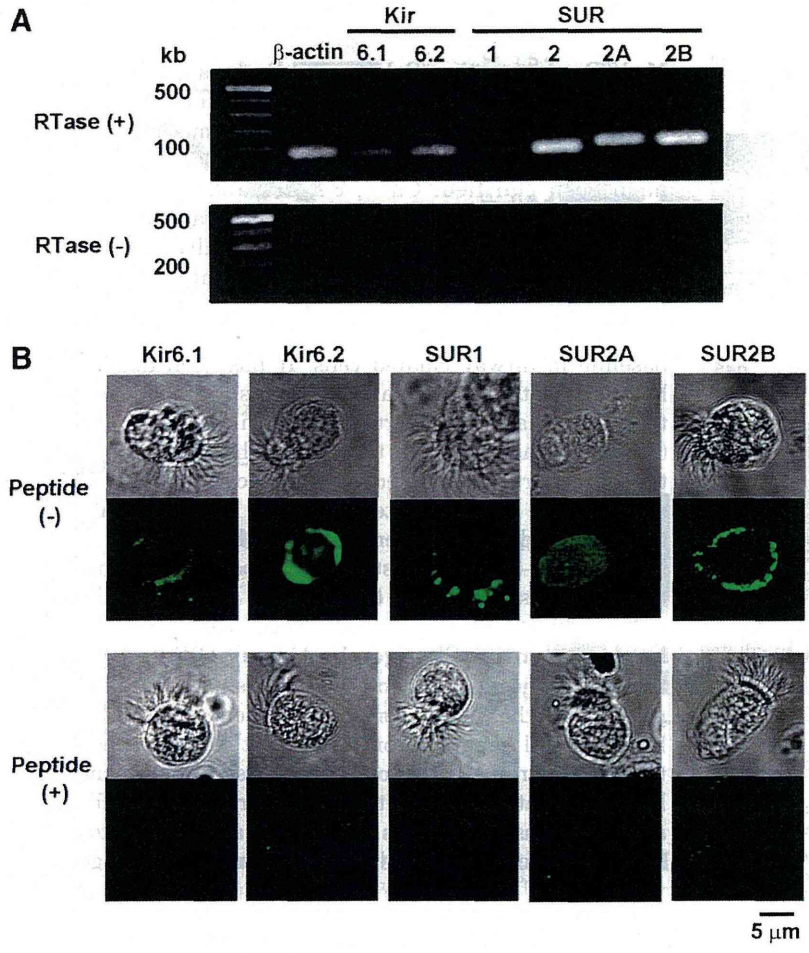


**Fig. 4.** The expression of $K_{ATP}$ channel mRNA and protein in the ciliated cells. (A) The expression of Kir6.x and SURx in the ciliated cells was examined by multi-cell reverse-transcription PCR. Approximately 40 of the isolated ciliated cells in which ciliary movement was detected were collected by small pipettes in microscopic fields. Reaction solution from which RTase was omitted was used as a negative control. The expression of the transcripts for Kir6.1, Kir6.2 and SUR2 was detected. Further analyses suggest that the major transcript of SUR2 was SUR2B. (B) The protein expression was detected using immunocytochemical staining. Similarly to the results from RT-PCR, Kir6.1, Kir6.2, and SUR2B but not SUR2A were expressed on cell surface. SUR1 exhibited specific expression on cilia. The lower sets of panels indicate that the specific staining was prevented by a corresponding inhibitory peptide.

attributed to $[Ca^{2+}]_i$ rise by membrane hyperpolarization induced under voltage-clamp or by application of a $K_{ATP}$ channel opener.

Previous studies have confirmed that the rise of $[Ca^{2+}]_i$ results in CBF enhancement, even if the underlying mechanisms are not fully understood (Schmid and Salathe, 2011). The activation of calmodulin may be involved, as this messenger protein associates with the radial spokes and the central apparatus of the flagella (Dymek and Smith, 2007) and directly interacts with dynein arms (Sakato et al., 2007). These mechanisms have been suggested for correlating the $[Ca^{2+}]_i$ rise with facilitated axoneme motility in invertebrates. In addition, it has been assumed that the $[Ca^{2+}]_i$ rise facilitates cilia motility via crosstalk with the cAMP or the cGMP mediated pathways (Braiman and Priel, 2008).

**$Ca^{2+}$ Source and Local $Ca^{2+}$ Functions in the Regulation of Cilia Motility.** In airway ciliated cells, it has been well established that two major endogenous stimulants, ATP and acetylcholine, activate $P_2Y_2$ and $M_3$ receptors, respectively. The stimuli activates phospholipase C$\beta$ to form inositol 1,4,5 trisphosphate, which induces $[Ca^{2+}]_i$ release from the endoplasmic reticulum. In addition, sustained $Ca^{2+}$ influx has been found to occur after $Ca^{2+}$ release. Although the molecular mechanism of the $Ca^{2+}$ influx is not well understood, the store-operated or receptor-operated $Ca^{2+}$ entry may be contributing as it does in many other non-excitable cells. By some stimuli, such as stretch, the transient receptor potential vanilloid subfamily 4 (TRPV4) channel is activated to facilitate $Ca^{2+}$ influx (Lorenzo et al., 2008).

In the present study, membrane hyperpolarization by voltage-clamp or the application of a $K_{ATP}$ channel opener has been clearly shown to facilitate the influx of $Ca^{2+}$. Because airway epithelial cells are polarized structures with cilia on their apical membranes, $Ca^{2+}$ concentrations are sufficiently high in the submembranous areas to affect ciliary beat (Braiman and Priel, 2008). It has been suggested that storage and release of $Ca^{2+}$ in different cell compartments give rise to this apical versus basolateral concentration difference in the cytosol (Braiman et al., 2000; Braiman and Priel, 2001). In contrast, the measurement of the local $[Ca^{2+}]_i$ in this study did not show a significant $Ca^{2+}$ gradient in the cytosol under the normal conditions (not shown). During membrane hyperpolarization by $K_{ATP}$ openers, the $Ca^{2+}$ rise in the apical submembrane area was significantly higher than that in the center area but not in the basolateral area.

In addition to a $Ca^{2+}$ rise in the apical region, diazoxide occasionally induced a slower $Ca^{2+}$ rise in the cytosolic compartments located deep inside the cells. Diazoxide reportedly interacts with the mitochondrial $K_{ATP}$ channels as well as with plasma membrane $K_{ATP}$ channels (Garlid et al., 1996; O'Rourke, 2004). Diazoxide reduces the mitochondrial membrane potential (or induces the mitochondrial depolarization) and thereby accelerates the release of $Ca^{2+}$ from mitochondria (Grimmsmann and Rustenbeck, 1998; Holmuhamedov

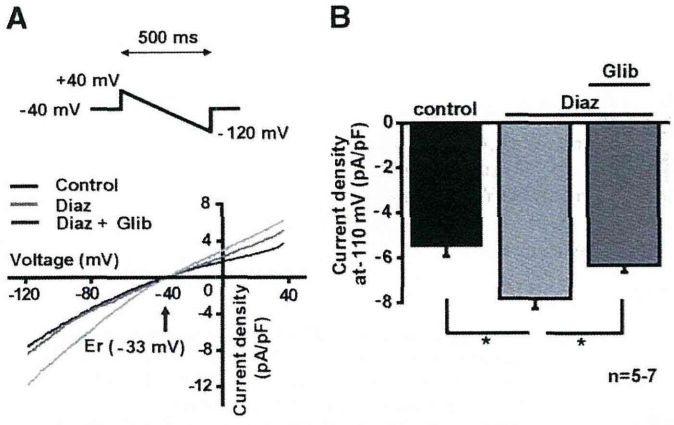


**Fig. 5.** $K_{ATP}$ current in ciliated cells. (A) The membrane currents were measured from a single ciliary cell under a voltage-clamp. A ramp pulse from +40 to −120 mV (as indicated in inset) was applied in the absence (control) and the presence of 10 $\mu$M diazoxide (Diaz) and following the addition of 5 $\mu$M glibenclamide (Glib). The I-V relationships were obtained by the ramp pulse protocol. The I-V relationships in the presence of diazoxide with the absence and presence of glibenclamide crossed at −33 mV. (B) The data concerning the current density at −110 mV were summarized. The numbers of experiments were seven in the control, seven in the presence of diazoxide, and five in the co-presence of glibenclamide. *$P < 0.05$.

et al., 1999). In addition to the $Ca^{2+}$ influx mediated by the membrane hyperpolarization, the release of $Ca^{2+}$ from organelles, including mitochondria, may be involved in the diazoxide-induced $Ca^{2+}$ increase. However, it remains to be determined whether the $Ca^{2+}$ rise induced by diazoxide deep inside the cell compartments contributes to the enhancement of the ciliary movement. Further experiments are therefore required to elucidate the mechanism underlying the local $Ca^{2+}$ mobilization triggered by exposure to diazoxide.

**$K_{ATP}$ Channels in Ciliated Cells as a Possible Therapeutic Target.** $K^+$ channels play a major role in maintaining the electrochemical gradient necessary for transepithelial $Na^+$ and $Cl^-$ transport in secretory airway epithelia (O'Grady and Lee, 2003). The $K_{ATP}$ channel is believed to be a significant contributor to lung physiology and pathophysiology because of the beneficial actions of openers in the lung (Fukuse et al., 2002). The molecular components of the $K_{ATP}$ channel in the airway alveolar epithelial type II cells of the rat have been identified as the combination of Kir6.1 and SUR2B (Leroy et al., 2004). A $K_{ATP}$ channel opener induces the relaxation of airway smooth muscle via membrane hyperpolarization and the subsequent suppression of voltage-dependent $Ca^{2+}$ channel (VDCC) activity (Rodrigo and Standen, 2005). This relaxation is considered to be effective for the therapy of occlusive diseases, such as asthma and chronic obstructive pulmonary disease (Pelaia et al., 2002).

In this study, two $K_{ATP}$ channel openers, diazoxide and pinacidil, and the $K_{ATP}$ channel blocker glibenclamide were used as pharmacological tools to determine the subunits responsible for $K_{ATP}$ channel activation in mouse ciliated cells. The combination of $K_{ATP}$ channel subunits modulates sensitivity to $K_{ATP}$ channel openers. Diazoxide activates SUR1 and SUR2B but not SUR2A (Yamada and Kurachi, 2005). On the other hand, pinacidil activates SUR2A and SUR2B but not SUR1. Because $K_{ATP}$ channels in ciliated cells were activated by both diazoxide and pinacidil at <10 $\mu$M, functional $K_{ATP}$ channels in these cells are supposed to be Kir6.x/SUR2B (Hibino et al., 2010). These results were supported by the outcomes from reverse-transcription PCR analyses and immunocytochemical staining, which showed the expression of Kir6.1, Kir6.2, and SUR2B on plasma membrane. It is interesting that immunostaining using anti-SUR1 revealed that SUR1 subunits were specifically located on cilia, but neither Kir6.1 nor Kir6.2 was detected there. SUR1 may possibly couple with other ion channels, such as the transient receptor potential channel (Woo et al., 2013). Unfortunately, the strategy of molecular manipulation by use of siRNA did not fit to this study because rat cilia disappear during cell culture for 2 days (Chang et al., 1985); the results were

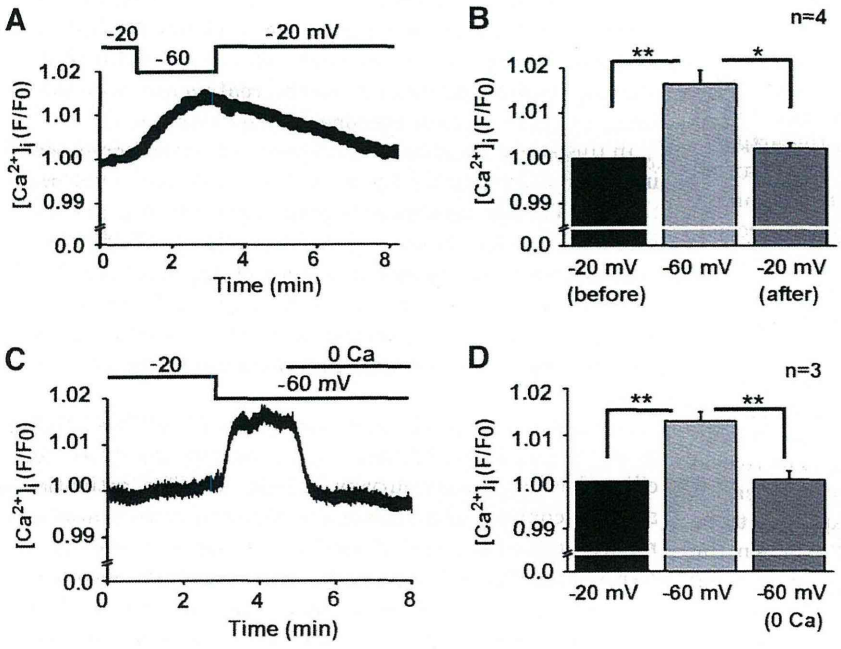


**Fig. 6.** $[Ca^{2+}]_i$ changes induced by the membrane hyperpolarization in ciliary the cells under a voltage-clamp. (A) The changes in $[Ca^{2+}]_i$ were monitored with the $F/F_0$ of the fluo4 that was applied from the recording pipette. The time course of $F/F_0$ during the membrane potential changes from −20 mV to −60 mV and back to −20 mV was plotted against time. The top trace indicates the clamp potential changes. (B) The summarized data concerning $F/F_0$ at −20 mV, at −60 mV, and back to −20 mV are shown ($n = 4$). *,**$P <$ 0.05 and 0.01, respectively. (C) The effect of $Ca^{2+}$ removal from an external solution on the elevated $F/F_0$ by the hyperpolarization of the membrane was examined in a ciliary cell under a voltage clamp. The external solution was exchanged from the standard solution (2.2 mM $Ca^{2+}$) to a $Ca^{2+}$ free solution (0 mM $Ca^{2+}$) at a potential of −60 mV as indicated in the top trace. (D) The summarized data concerning $F/F_0$ at −20 mV at −60 mV and following the exposure to a $Ca^{2+}$ free solution are shown ($n = 4$). *,**$P < 0.05$ and 0.01, respectively.

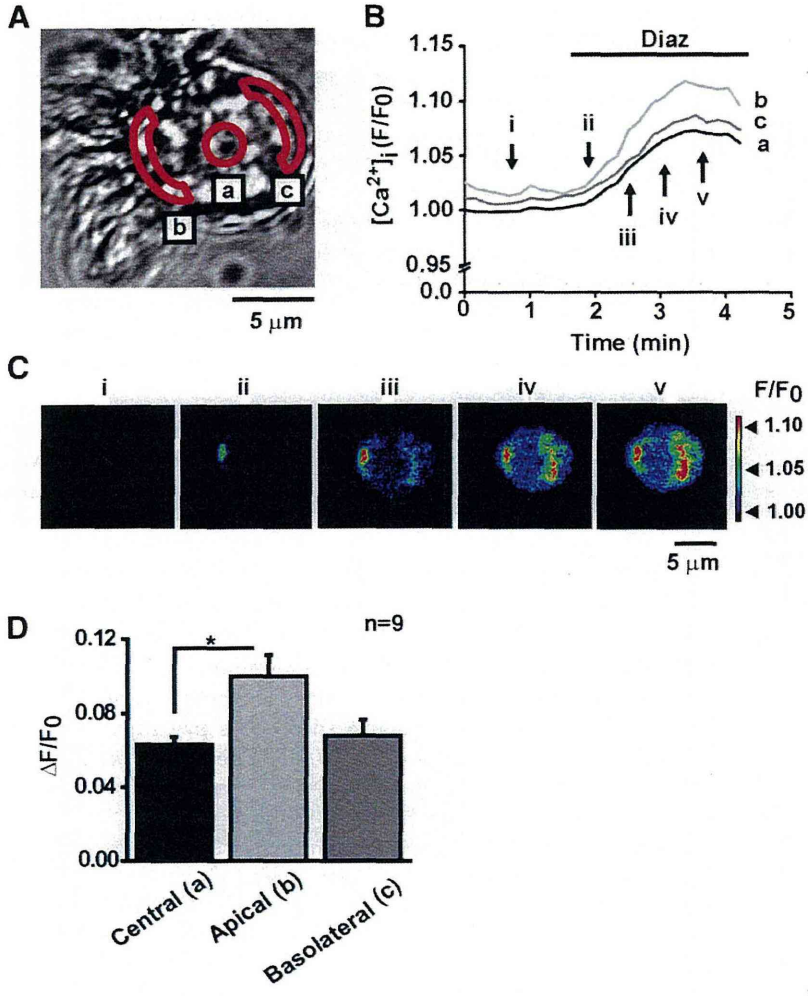


**Fig. 7.** The image analyses of local $Ca^{2+}$ transients induced by diazoxide in the ciliary cells. (A) The local $Ca^{2+}$ transients were measured by confocal fluorescent microscopy. The $F/F_0$ signals of fluo-4 were measured in the three areas indicated in the transfer image of the ciliary cell: "a" (center of the cell). "b" (apical submembrane area), and "c" (basolateral submembrane area). (B) Changes in $F/F_0$ in the three areas were plotted against time. The $F_0$ in area "a" was taken as 1.0 and $F/F_0$ in the other areas was normalized by the $F_0$. (C) The confocal images of $[Ca^{2+}]_i$ were obtained from the ciliary cell in the absence (i) and presence (ii, iii, and iv) of diazoxide at the timing shown in B. (D) The summarized data concerning $\Delta F/F_0$ were obtained as the differences of $F/F_0$ in the absence and presence of diazoxide in B ($n = 9$). *$P < 0.05$.

confirmed using mouse cilia in this study. Therefore, it remains to be determined whether Kir6.1 or Kir6.2 is the functionally predominant subunit in ciliated cells, whereas Kir6.2 protein expression on the plasma membrane appeared to be higher than Kir6.1.

Membrane potential recording with $DiBAC_4(3)$ allows us to get more number of results than the direct recordings under whole-cell patch clamp configuration. However, the use of $DiBAC_4(3)$ has at least three limitations. First, the artifacts by $DiBAC_4(3)$ act as a potent activator of BK channel (Morimoto et al., 2007). BK channel current component sensitive to paxilline was not recorded in ciliary cells. Second, $DiBAC_4(3)$ cannot detect fast membrane potential changes. Third, the most serious limitation is that the exact membrane potential cannot be measured by $DiBAC_4(3)$, even though calibration under voltage-clamp is available (Yamada et al., 2001). The membrane hyperpolarization induced by 10 $\mu$M diazoxide appeared to be approximately 11 mV based on the calibration. This value was apparently larger than that directly recorded under current-clamp mode (4 mV). The reason for the dissociation between two measurements is not clear. It is, however, likely that the $Cl^-$ conductance appears to be high compared with that of $K^+$ in ciliated cells. When the pipette filling solution contained 140 mM $Cl^-$, the resting membrane potential was extremely shallow (−19 mV) and close to equilibrium potential of $Cl^-$ rather than $K^+$. Under these experimental conditions, the membrane hyperpolarization attributed to the $K^+$ conductance increase may be smaller than what occurs under normal $Cl^-$ gradient across the cell membrane. The intracellular $Cl^-$ concentration varied widely depending on cell types in a range of 5 and 30 mM but is unfortunately unknown in tracheal ciliated cells. Further study is required to understand the real membrane hyperpolarization by $K_{ATP}$ channel opening in ciliary cells.

In this study, the membrane hyperpolarization increased the influx of $Ca^{2+}$ presumably by an unknown pathway rather than by VDCC. The membrane hyperpolarization may simply increase the transmembrane driving force for $Ca^{2+}$ through $Ca^{2+}$ permeable channels with non–voltage-dependent gating mechanisms. Taken together, it can be suggested that $K_{ATP}$ channel openers may have additional benefits, including an expectorant effect, for the therapy of occlusive respiratory disorders.

In conclusion, a $K_{ATP}$ channel composed of Kir6.2/SUR2B and possibly also Kir6.1/SUR2B is functionally expressed in ciliated cells in mice airway epithelium. The activation of a $K_{ATP}$ channel induces membrane hyperpolarization and results in an increase in $Ca^{2+}$-influx through a novel, non-VDCC pathway. The enhancement of the ciliary movement by $K_{ATP}$ openers is mainly attributable to the $Ca^{2+}$ rise and is considered to have an additional and beneficial effect on the

current drug therapies used to treat occlusive respiratory disorders.

### Authorship Contributions

*Participated in research design*: Ohba, Sawada, Imaizumi.

*Conducted experiments*: Ohba, Sawada, Suzuki.

*Performed data analysis*: Ohba, Sawada, Yamamura, Ohya, Imaizumi.

*Wrote or contributed to the writing of the manuscript*: Tsuda, Imaizumi.

### References


Braiman A, Gold'Shtein V, and Priel Z (2000) Feasibility of a sustained steep $Ca^{2+}$ Gradient in the cytosol of electrically non-excitable cells. *J Theor Biol* **206**:115–130.

Braiman A and Priel Z (2001) Intracellular stores maintain stable cytosolic $Ca^{2+}$ gradients in epithelial cells by active $Ca^{2+}$ redistribution. *Cell Calcium* **30**:361–371.

Braiman A and Priel Z (2008) Efficient mucociliary transport relies on efficient regulation of ciliary beating. *Respir Physiol Neurobiol* **163**:202–207.

Chang LY, Wu R, and Nettesheim P (1985) Morphological changes in rat tracheal cells during the adaptive and early growth phase in primary cell culture. *J Cell Sci* **74**:283–301.

Clark R and Proks P (2010) ATP-sensitive potassium channels in health and disease. *Adv Exp Med Biol* **654**:165–192.

Dymek EE and Smith EF (2007) A conserved CaM- and radial spoke associated complex mediates regulation of flagellar dynein activity. *J Cell Biol* **179**:515–526.

Evans JH and Sanderson MJ (1999) Intracellular calcium oscillations regulate ciliary beat frequency of airway epithelial cells. *Cell Calcium* **26**:103–110.

Flagg TP, Enkvetchakul D, Koster JC, and Nichols CG (2010) Muscle $K_{ATP}$ channels: recent insights to energy sensing and myoprotection. *Physiol Rev* **90**:799–829.

Fukuse T, Hirata T, Omasa M, and Wada H (2002) Effect of adenosine triphosphate-sensitive potassium channel openers on lung preservation. *Am J Respir Crit Care Med* **165**:1511–1515.

Funabashi K, Ohya S, Yamamura H, Hatano N, Muraki K, Giles W, and Imaizumi Y (2010) Accelerated $Ca^{2+}$ entry by membrane hyperpolarization due to $Ca^{2+}$-activated $K^+$ channel activation in response to histamine in chondrocytes. *Am J Physiol Cell Physiol* **298**:C786–C797.

Garlid KD, Paucek P, Yarov-Yarovoy V, Sun X, and Schindler PA (1996) The mitochondrial $K_{ATP}$ channel as a receptor for potassium channel openers. *J Biol Chem* **271**:8796–8799.

Grimmsmann T and Rustenbeck I (1998) Direct effects of diazoxide on mitochondria in pancreatic β-cells and on isolated liver mitochondria. *Br J Pharmacol* **123**: 781–788.

Hibino H, Inanobe A, Furutani K, Murakami S, Findlay I, and Kurachi Y (2010) Inwardly rectifying potassium channels: their structure, function, and physiological roles. *Physiol Rev* **90**:291–366.

Holmuhamedov EL, Wang L, and Terzic A (1999) ATP-sensitive $K^+$ channel openers prevent $Ca^{2+}$ overload in rat cardiac mitochondria. *J Physiol* **519**:347–360.

Imaizumi Y, Muraki K, and Watanabe M (1989) Ionic currents in single smooth muscle cells from the ureter of the guinea-pig. *J Physiol* **411**:131–159.

Kawakami M, Nagira T, Hayashi T, Shimamoto C, Kubota T, Mori H, Yoshida H, and Nakahari T (2004) Hypo-osmotic potentiation of acetylcholine-stimulated ciliary beat frequency through ATP release in rat tracheal ciliary cells. *Exp Physiol* **89**:739–751.

Leroy C, Dagenais A, Berthiaume Y, and Brochiero E (2004) Molecular identity and function in transepithelial transport of $K_{ATP}$ channels in alveolar epithelial cells. *Am J Physiol Lung Cell Mol Physiol* **286**:L1027–L1037.

Lorenzo IM, Liedtke W, Sanderson MJ, and Valverde MA (2008) TRPV4 channel participates in receptor-operated calcium entry and ciliary beat frequency regulation in mouse airway epithelial cells. *Proc Natl Acad Sci USA* **105**:12611–12616.

Ma W, Silberberg SD, and Priel Z (2002) Distinct axonemal processes underlie spontaneous and stimulated airway ciliary activity. *J Gen Physiol* **120**:875–885.

Malerba M, Radaeli A, Mancuso S, and Polosa R (2010) The potential therapeutic role of potassium channel modulators in asthma and chronic obstructive pulmonary disease. *J Biol Regul Homeost Agents* **24**:123–130.

Morimoto T, Sakamoto K, Sade H, Ohya S, Muraki K, and Imaizumi Y (2007) Voltage-sensitive oxonol dyes are novel large-conductance $Ca^{2+}$-activated $K^+$ channel activators selective for β1 and β4 but not for β2 subunits. *Mol Pharmacol* **71**:1075–1088.

O'Grady SM and Lee SY (2003) Chloride and potassium channel function in alveolar epithelial cells. *Am J Physiol Lung Cell Mol Physiol* **284**:L689–L700.

O'Rourke B (2004) Evidence for mitochondrial $K^+$ channels and their role in cardioprotection. *Circ Res* **94**:420–432.

Pelaia G, Gallelli L, Vatrella A, Grembiale RD, Maselli R, De Sarro GB, and Marsico SA (2002) Potential role of potassium channel openers in the treatment of asthma and chronic obstructive pulmonary disease. *Life Sci* **70**:977–990.

Rodrigo GC and Standen NB (2005) ATP-sensitive potassium channels. *Curr Pharm Des* **11**:1915–1940.

Sakato M, Sakakibara H, and King SM (2007) Chlamydomonas outer arm dynein alters conformation in response to $Ca^{2+}$. *Mol Biol Cell* **18**:3620–3634.

Salathe M (2007) Regulation of mammalian ciliary beating. *Annu Rev Physiol* **69**: 401–422.

Salathe M and Bookman RJ (1999) Mode of $Ca^{2+}$ action on ciliary beat frequency in single ovine airway epithelial cells. *J Physiol* **520**:851–865.

Schmid A and Salathe M (2011) Ciliary beat co-ordination by calcium. *Biol Cell* **103**: 159–169.

Seybold ZV, Mariassy AT, Stroh D, Kim CS, Gazeroglu H, and Wanner A (1990) Mucociliary interaction in vitro: effects of physiological and inflammatory stimuli. *J Appl Physiol* **68**:1421–1426.

Shiima-Kinoshita C, Min KY, Hanafusa T, Mori H, and Nakahari T (2004) β2-adrenergic regulation of ciliary beat frequency in rat bronchiolar epithelium: potentiation by isosmotic cell shrinkage. *J Physiol* **554**:403–416.

Tarasiuk A, Bar-Shimon M, Gheber L, Korngreen A, Grossman Y, and Priel Z (1995) Extracellular ATP induces hyperpolarization and motility stimulation of ciliary cells. *Biophys J* **68**:1163–1169.

Trinh NT, Privé A, Kheir L, Bourret JC, Hijazi T, Amraei MG, Noël J, and Brochiero E (2007) Involvement of $K_{ATP}$ and KvLQT1 $K^+$ channels in EGF-stimulated alveolar epithelial cell repair processes. *Am J Physiol Lung Cell Mol Physiol* **293**:L870–L882.

Trinh NT, Privé A, Maillé E, Noël J, and Brochiero E (2008) EGF and $K^+$ channel activity control normal and cystic fibrosis bronchial epithelia repair. *Am J Physiol Lung Cell Mol Physiol* **295**:L866–L880.

Weiss T, Gheber L, Shoshan-Barmatz V, and Priel Z (1992) Possible mechanism of ciliary stimulation by extracellular ATP: involvement of calcium-dependent potassium channels and exogenous $Ca^{2+}$. *J Membr Biol* **127**:185–193.

Woo SK, Kwon MS, Ivanov A, Gerzanich V, and Simard JM (2013) The sulfonylurea receptor 1 (Sur1)-transient receptor potential melastatin 4 (Trpm4) channel. *J Biol Chem* **288**:3655–3667.

Yamada A, Gaja N, Ohya S, Muraki K, Narita H, Ohwada T, and Imaizumi Y (2001) Usefulness and limitation of $DiBAC_4(3)$, a voltage-sensitive fluorescent dye, for the measurement of membrane potentials regulated by recombinant large conductance $Ca^{2+}$-activated $K^+$ channels in HEK293 cells. *Jpn J Pharmacol* **86**:342–350.

Yamada M and Kurachi Y (2005) A functional role of the C-terminal 42 amino acids of SUR2A and SUR2B in the physiology and pharmacology of cardiovascular ATP-sensitive $K^+$ channels. *J Mol Cell Cardiol* **39**:1–6.

Yamamura H, Ikeda C, Suzuki Y, Ohya S, and Imaizumi Y (2012) Molecular assembly and dynamics of fluorescent protein-tagged single $K_{Ca}1.1$ channel in expression system and vascular smooth muscle cells. *Am J Physiol Cell Physiol* **302**: C1257–C1268.

Yamazaki D, Kito H, Yamamoto S, Ohya S, Yamamura H, Asai K, and Imaizumi Y (2011) Contribution of $K_ir2$ potassium channels to ATP-induced cell death in brain capillary endothelial cells and reconstructed HEK293 cell model. *Am J Physiol Cell Physiol* **300**:C75–C86.


**Address correspondence to:** Dr. Yuji Imaizumi, Department of Molecular and Cellular Pharmacology, Graduate School of Pharmaceutical Sciences, Nagoya City University, 3-1 Tanabedori, Mizuhoku, Nagoya 467-8603, Japan. E-mail: yimaizum@phar.nagoya-cu.ac.jp

*Materials* **2013**, *6*, 2713-2722; doi:10.3390/ma6072713

OPEN ACCESS

*materials*

**ISSN 1996-1944**

www.mdpi.com/journal/materials

*Article*

# Cytotoxic Effects of Hydroxylated Fullerenes in Three Types of Liver Cells

**Kumiko Shimizu [1,*], Reiji Kubota [1], Norihiro Kobayashi [1], Maiko Tahara [1], Naoki Sugimoto [2], Tetsuji Nishimura [1,3] and Yoshiaki Ikarashi [1]**

[1] Division of Environmental Chemistry, National Institute of Health Sciences, Kamiyoga 1-18-1, Setagaya-ku, Tokyo 158-8501, Japan; E-Mails: reijik@nihs.go.jp (R.K.); norihiro.kobayashi@nihs.go.jp (N.K.); tahara@nihs.go.jp (M.T.); ikarashi@nihs.go.jp (Y.I.)

[2] Division of Food Additives, National Institute of Health Sciences, Kamiyoga 1-18-1, Setagaya-ku, Tokyo 158-8501, Japan; E-Mail: nsugimot@nihs.go.jp

[3] Faculty of Pharmaceutical Sciences, Teikyo Heisei University, Uruidominami 4-1, Ichihara-shi, Chiba 290-0193, Japan; E-Mail: t.nishimura@thu.ac.jp

* Author to whom correspondence should be addressed; E-Mail: kshimizu@nihs.go.jp; Tel./Fax: +81-3-3700-9304.

*Received: 27 April 2013; in revised form: 17 June 2013 / Accepted: 2 July 2013 / Published: 9 July 2013*

**Abstract:** Fullerenes $C_{60}$ have attracted considerable attention in the biomedical field due to their interesting properties. Although there has been a concern that $C_{60}$ could be metabolized to hydroxylated fullerenes ($C_{60}(OH)_x$) *in vivo*, there is little information on the effect of hydroxylated $C_{60}$ on liver cells. In the present study, we evaluated the cytotoxic effects of fullerene $C_{60}$ and various hydroxylated $C_{60}$ derivatives, $C_{60}(OH)_2$, $C_{60}(OH)_{6-12}$, $C_{60}(OH)_{12}$ and $C_{60}(OH)_{36}$, with three different types of liver cells, dRLh-84, HepG2 and primary cultured rat hepatocytes. $C_{60}$, $C_{60}(OH)_2$ and $C_{60}(OH)_{36}$ exhibited little or no cytotoxicity in all of the cell types, while $C_{60}(OH)_{6-12}$ and $C_{60}(OH)_{12}$ induced cytotoxic effects in dRLh-84 cells, accompanied by the appearance of numerous vacuoles around the nucleus. Moreover, mitochondrial activity in liver cells was significantly inhibited by $C_{60}(OH)_{6-12}$ and $C_{60}(OH)_{12}$. These results indicate that the number of hydroxyl groups on $C_{60}(OH)_x$ contribute to the difference of their cytotoxic potential and mitochondrial damage in liver cells.

**Keywords:** hydroxylated fullerene; $C_{60}$; cytotoxic activity; liver cells; mitochondrial damage

## 1. Introduction

Fullerene $C_{60}$ is comprised of 12 five-membered rings and 20 six-membered rings (Figure 1) [1]. The high chemical stability of fullerenes resists the potential metabolic degradation associated with the carbon cage-opening process under the biological conditions [2–4]. Since its discovery in 1985 [5], nanomaterials are applied in various fields due to those useful properties. Fullerene $C_{60}$ and derivatives have anti-cancer and neuroprotective properties as a consequence of antioxidant and free-radical scavenger activity both *in vitro* and *in vivo* [6–10], as well as photo-induced DNA cleavage ability [11]. Moreover, derivatives of fullerene $C_{60}$ have been demonstrated to act as HIV-1 protease inhibitors, which have started to be evaluated in clinical trials [12]. Thus, fullerene $C_{60}$ and its derivatives are expected to have potential applications in the life and medical sciences. However, the insolubility of $C_{60}$ and $C_{70}$ in aqueous solution makes such studies difficult.

Several studies have reported the biodistribution of $C_{60}$ in various experimental animals [13–16]. We have also reported that the accumulation and decreased concentration of $C_{60}$ in various tissues such as lung, liver, kidney, brain, *etc.*, indicate the possibility of $C_{60}$ and $C_{60}$ metabolites being excreted into feces and/or urine [17]. If it is assumed that $C_{60}$ undergoes *in vivo* enzymatic metabolism in the liver, $C_{60}$ oxidation products such as hydroxylated fullerenes ($C_{60}(OH)_x$) may be produced. At present, the bioavailability of $C_{60}(OH)_x$ has begun to garner attention. In human epidermal keratinocyte (HEK) cells, $C_{60}(OH)_{32}$ has shown significant cytotoxic activity [18]. Moreover, $C_{60}(OH)_{22-26}$ has been shown to induce phototoxicity in human retinal pigment epithelial cells [19]. Yamasaki *et al.* (2006) reported that $C_{60}(OH)_{24}$ induced cytotoxicity in human umbilical vein endothelial cells [20]. Nakagawa *et al.* reported that $C_{60}(OH)_{24}$ showed cytotoxicity to isolated rat hepatocyte cells [21]. These studies were performed using $C_{60}(OH)_x$ containing 22–32 hydroxyl groups, although it is thought that $C_{60}(OH)_x$ produced in the metabolic process has a low number of hydroxyl groups. No information has been obtained about the cytotoxic effects of $C_{60}(OH)_x$ with a low number of hydroxyl groups in liver cells. Insufficient information is available about the cytotoxicity mechanisms of hydroxylated $C_{60}$ in liver cells. Furthermore, considering the metabolization and adverse effects of anti-cancer drugs and anti-HIV medicines containing fullerene derivatives, the information of the cytotoxic activities of $C_{60}(OH)_x$ at the liver is very important.

In the present study, we investigated the cytotoxic effects of $C_{60}$ and the hydroxylated fullerenes, $C_{60}(OH)_2$, $C_{60}(OH)_{6-12}$, $C_{60}(OH)_{12}$ and $C_{60}(OH)_{36}$ to three types of liver cells, primary cultured rat hepatocytes, dRLh-84 and HepG2. Primary cultured rat hepatocytes maintain phase I, II metabolic activity and uptake transporter activity. dRLh-84 and HepG2 are rat and human hepatoma cells, which have no metabolic activity and were used to evaluate species-differences between rats and humans.

## 2. Results

### *2.1. Mass Spectrometric Analysis of $C_{60}(OH)_x$*

Figure 1 shows chemical formulas of $C_{60}$ and $C_{60}(OH)_x$. The positions which hydroxyl groups of $C_{60}(OH)_{6-12 \text{ and } 36}$ substituted are uncertain.

$C_{60}(OH)_{6-12 \text{ and } 36}$ $C_{60}$ and $C_{60}(OH)_2$ samples showed one signal at $m/z$ = 720 and $m/z$ = 754, respectively (data not shown). Five mass spectrometric signals for $C_{60}(OH)_{12}$ were observed at

*m/z* = 821, 855, 889, 923 and 958. The major ion with *m/z* = 923 was assigned to $C_{60}(OH)_{12}$, and other ions with *m/z* = 821, 855, 889, and 958 were assigned to $C_{60}(OH)_6$, $C_{60}(OH)_8$, $C_{60}(OH)_{10}$, and $C_{60}(OH)_{14}$, respectively (Figure 2A). Mass spectrometric signals for $C_{60}(OH)_{6-12}$ are shown in Figure 2B. The major ion was assigned to $C_{60}(OH)_{10}$, and other ions were assigned to $C_{60}(OH)_6$, $C_{60}(OH)_8$, $C_{60}(OH)_{12}$ and $C_{60}(OH)_{14}$, respectively.

**Figure 1.** Chemical formulas of $C_{60}$ (**A**); $C_{60}(OH)_{6-12 \text{ or } 36}$ (**B**); and $C_{60}(OH)_2$ (**C**).

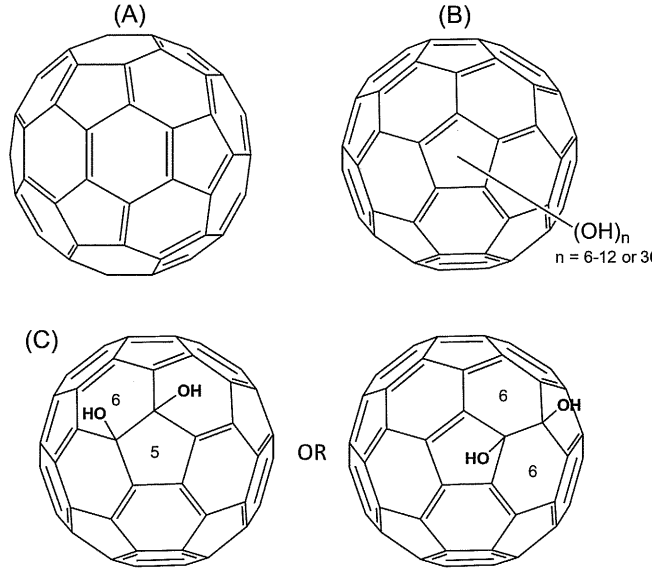


**Figure 2.** Mass Spectra of $C_{60}(OH)_{12}$ and $C_{60}(OH)_{6-12}$.

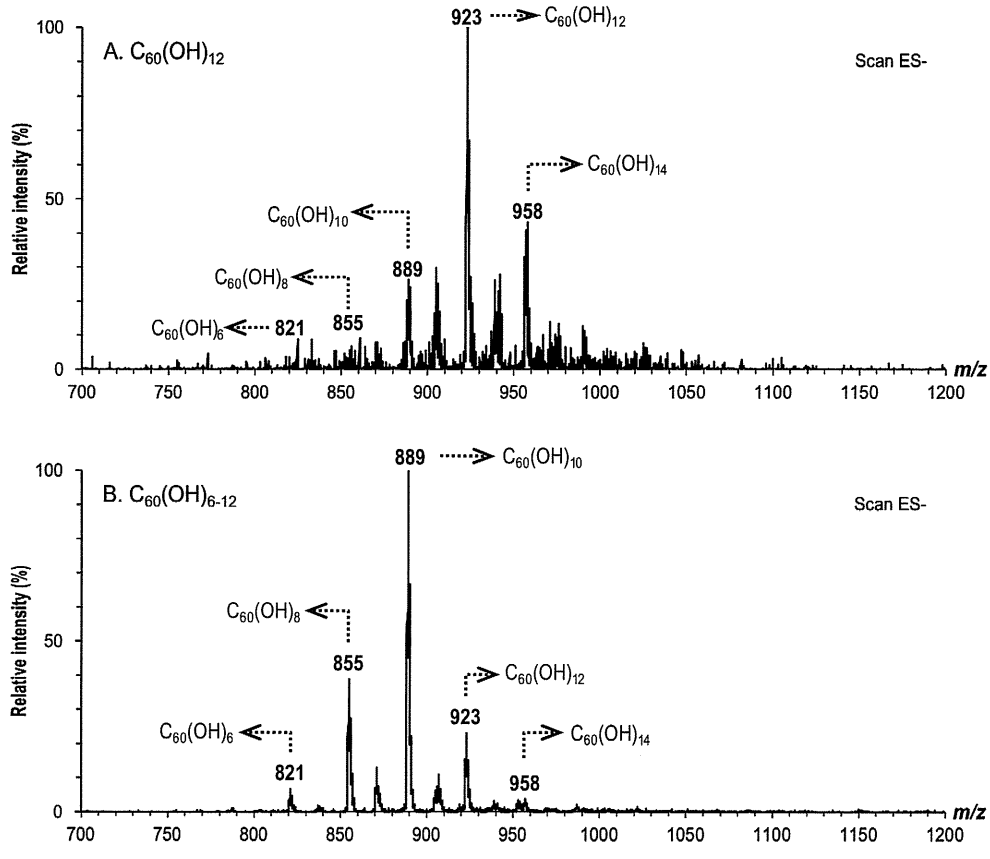

### *2.2. Cytotoxicity of $C_{60}$ and $C_{60}(OH)_x$*

Figure 3 shows cell survival curves of the three types of liver cells exposed to 0–100 μg/mL of $C_{60}$ and $C_{60}(OH)_x$. The maximum concentration was chosen considering suspension's turbidity and concentrations appeared toxic effects in previous studies [20–22]. Among the $C_{60}(OH)_x$ tested, $C_{60}(OH)_{6-12}$ had the most potent cytotoxic activity. In particular, $C_{60}(OH)_{6-12}$ and $C_{60}(OH)_{12}$ induced significant toxic activities in dRLh-84 with a dose dependent manner (Figure 3B). Exposure to $C_{60}(OH)_{6-12}$ and $C_{60}(OH)_{12}$ induced milder cytotoxicity in primary cultured rat hepatocytes than dRLh-84 (Figure 3C). In HepG2, $C_{60}(OH)_{6-12}$ showed toxic activity, which was lower than in dRLh-84. On the other hand, $C_{60}(OH)_{12}$ had weaker toxic activity in HepG2 than in dRLh-84 (Figure 3A,B). Other $C_{60}(OH)_x$ have little or no toxic effects.

**Figure 3.** Cytotoxicity of fullerene and hydroxylated fullerenes in liver cells after exposure for 3 days. HepG2 (**A**); dRLh-84 (**B**); and primary cultured rat hepatocytes (**C**) were exposed to $C_{60}$, $C_{60}(OH)_2$, $C_{60}(OH)_{6-12}$, $C_{60}(OH)_{12}$, and $C_{60}(OH)_{36}$ at concentrations of 0.3–100 μg/mL. After exposure, cytotoxicities were evaluated by the cell viability assay and the values are reported as % viability. Each data represents the mean ± SD ($n$ = 3). * Significantly different from the control: $p < 0.05$.

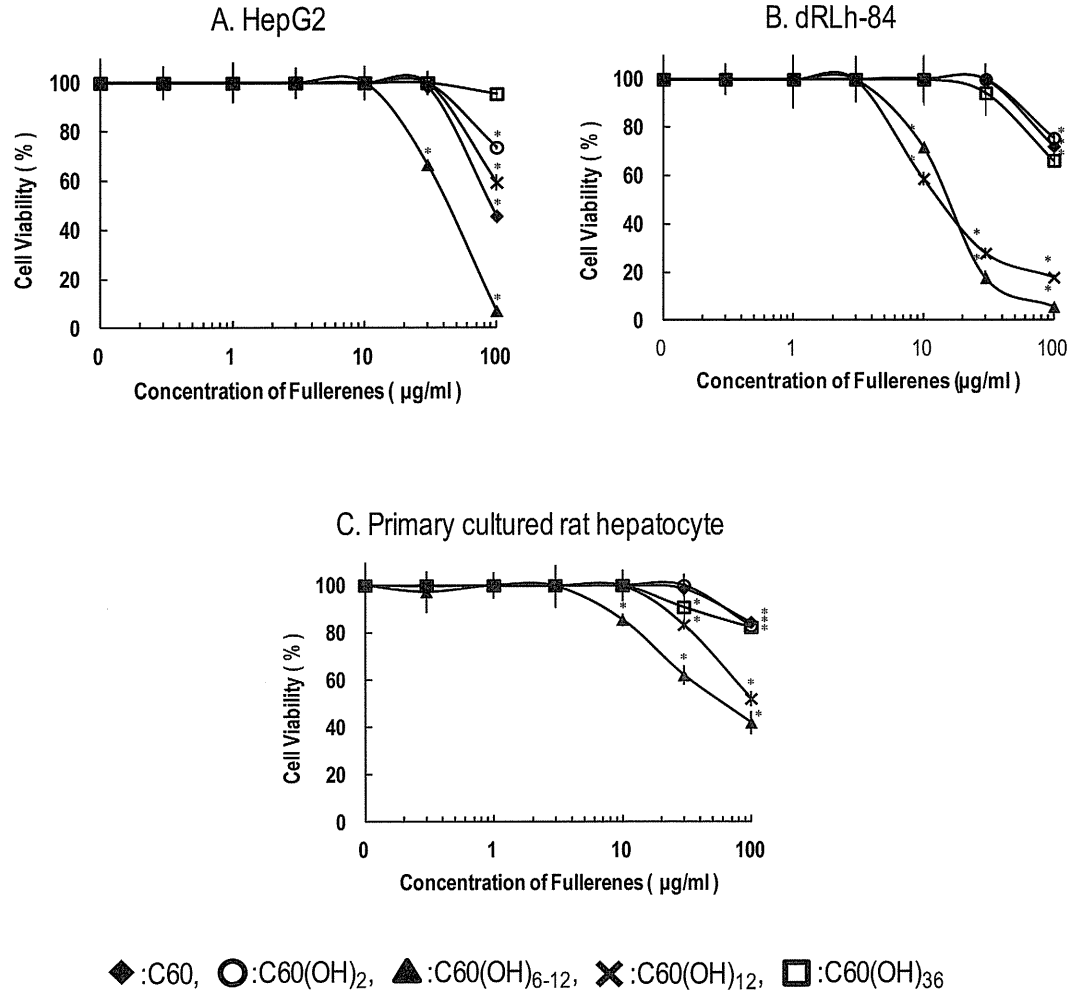

$C_{60}(OH)_{6-12}$ and $C_{60}(OH)_{12}$ at a concentration of 30 μg/mL caused the formation of numerous vacuoles around the nucleus in dRLh-84 cells (Figure 4). In contrast, the formation of cytoplasmic vacuoles was not detected in HepG2 and primary cultured rat hepatocytes (data not shown).

**Figure 4.** Numerous vacuoles of dRLh-84 cells treated with $C_{60}(OH)_{6-12}$ and $C_{60}(OH)_{12}$ for 24 h. After dRLh-84 cells were exposed to 30 μg/mL of $C_{60}(OH)_{6-12}$ and $C_{60}(OH)_{12}$, photographs were taken using an optical microscope. Scale bar: 50 μm. The arrows indicate cytoplasmic vacuoles.

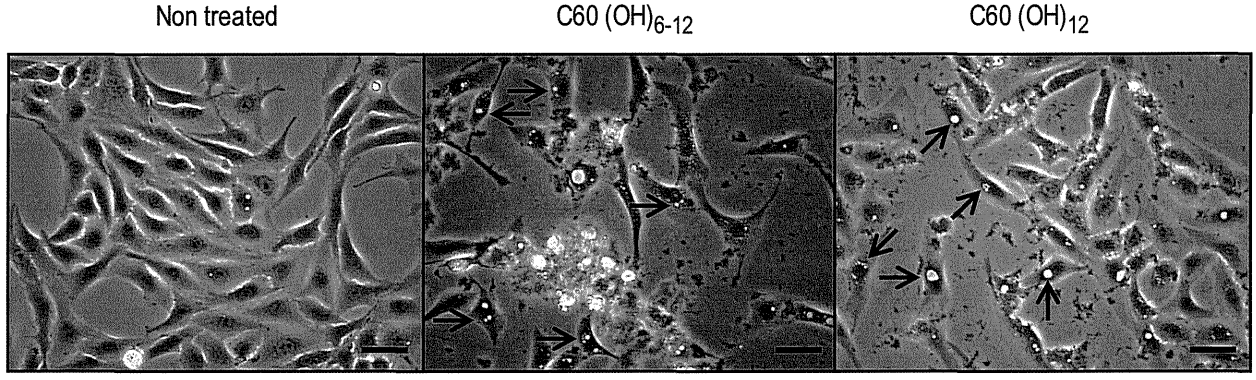


Mitochondrial succinate-tetrazolium reductase activity in all of the liver cells was inhibited by $C_{60}(OH)_{6-12}$ (Figure 5). $C_{60}(OH)_{12}$ also inhibited this enzymatic activity in dRLh-84, but provided little inhibition in HepG2 according to cytotoxic activities. The mitochondrial enzyme activity of primary cultured rat hepatocytes was also inhibited by $C_{60}(OH)_{6-12}$ and $C_{60}(OH)_{12}$ (Figure 5C). Other $C_{60}(OH)_x$ had almost a little or no effect.

**Figure 5.** Mitochondrial activity of fullerene and hydroxylated fullerenes in liver cells after exposure for 3 days. Three types of cells, HepG2 (**A**); dRLh-84 (**B**); and primary cultured rat hepatocytes (**C**) were treated with fullerene and hydroxylated fullerenes with the same concentrations as employed in the cell viability assay (the sample symbols are the same as in Figure 3). After exposure for 3 days, the inhibition rate (%) of mitochondrial activity was evaluated. Each data represents the mean ± SD ($n$ = 3). * Significantly different from the control: $p < 0.05$.

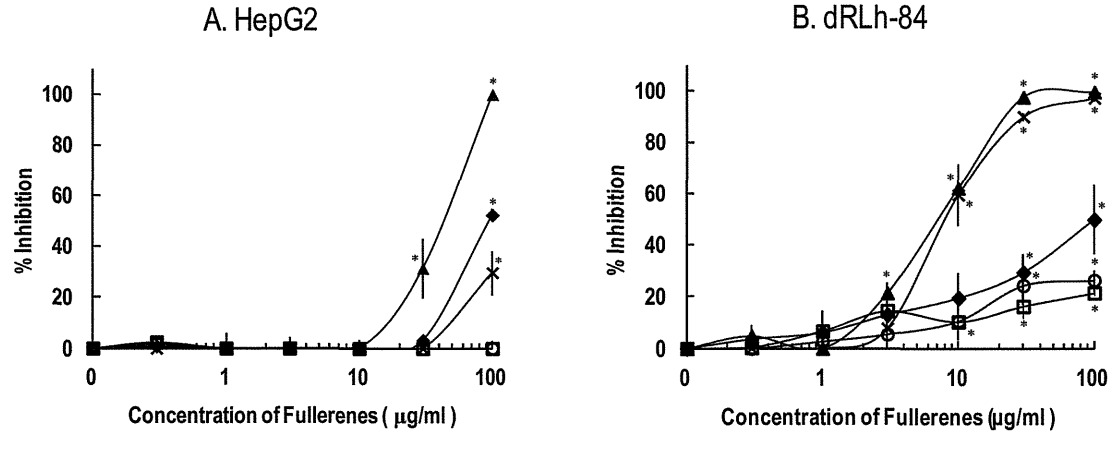

**Figure 5.** *Cont.*

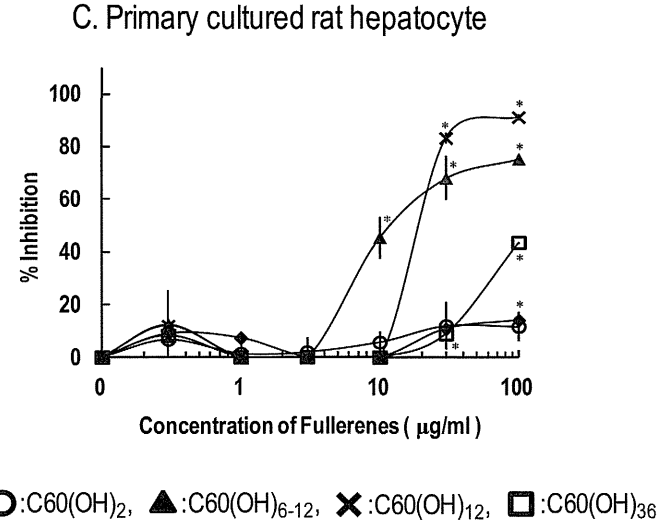


## 3. Discussion

The molecular diversity of $C_{60}(OH)_x$ samples used in this study was analyzed. Some of the molecular diversity of $C_{60}(OH)_{6–12}$ and $C_{60}(OH)_{12}$ showed overlapping distributions. $C_{60}(OH)_{36}$ had many constituents (data not shown). These results indicate that $C_{60}(OH)_x$ with the exception of $C_{60}(OH)_2$ contained various numbers of hydroxyl substituents. Because there is currently no purification technology available for $C_{60}(OH)_{x,\ x > 2,\ x < 12}$, it was impossible to separate single $C_{60}(OH)_{6,\ 8,\ 10}$ from $C_{60}(OH)_{6–12}$ and $C_{60}(OH)_{12}$.

The sensitivities of the three types of liver cells to $C_{60}(OH)_x$ differed (Figure 3). $C_{60}(OH)_{6–12}$ and $C_{60}(OH)_{12}$ exhibited more potent cytotoxic activity in dRLh-84 than in primary cultured rat hepatocytes. Primary cultured rat hepatocytes and dRLh-84 were from the same rat species, but the sensitivities to $C_{60}(OH)_{6–12}$ and $C_{60}(OH)_{12}$ were different. Thus, it was suspected that metabolic activity may affect the cytotoxicity of $C_{60}(OH)_{6–12}$ and $C_{60}(OH)_{12}$ in primary cultured rat hepatocytes.

Meanwhile, $C_{60}(OH)_{6–12}$ caused higher cytotoxic activity than $C_{60}(OH)_{12}$ in HepG2. In contrast, the cytotoxic activities between $C_{60}(OH)_{6–12}$ and $C_{60}(OH)_{12}$ show a slight difference. These results indicate that the interspecific difference in hepatoma cells may cause different sensitivities based on number of $C_{60}(OH)_x$ hydroxyl groups. Moreover, the malignant grade in the hepatoma might affect the sensitivity to the number of $C_{60}(OH)_x$ hydroxyl groups between dRLh-84 and HepG2.

While there was overlap in the components of $C_{60}(OH)_{6–12}$ and $C_{60}(OH)_{12}$, $C_{60}(OH)_{6–12}$ induced more severe cytotoxic activity than $C_{60}(OH)_{12}$ in all of the liver cells. $C_{60}(OH)_2$ and $C_{60}(OH)_{36}$ showed no cytotoxic effects in any liver cells. Although the number of hydroxyl groups that contribute to cytotoxicity cannot be specified, these results suggest that $C_{60}(OH)_6$, $C_{60}(OH)_8$, or/and $C_{60}(OH)_{10}$ would have more potent cytotoxic activity than other $C_{60}(OH)_x$. For a more detailed understanding, we would need to compare the cytotoxic potential, if it is possible to obtain the purified $C_{60}(OH)_6$, $C_{60}(OH)_8$ and $C_{60}(OH)_{10}$. Low numbers of $C_{60}$ hydroxyl substituents are expected to be generated by metabolism of $C_{60}$ in the liver after administration. Although the number of hydroxyl substituents

produced by hepatic metabolism cannot be identified, if 6–10 hydroxyl substituents were generated from $C_{60}$, cytotoxic activity induced in the hepatoma would be a concern.

Exposure to $C_{60}(OH)_{6-12}$ and $C_{60}(OH)_{12}$ resulted in the formation of numerous vacuoles around the nucleus in dRLh-84 (Figure 4). Several studies have also reported vacuole formation, or blebbing, upon exposure to $C_{60}(OH)_x$ [18,20,21,23]. Yamasaki *et al.* (2006) and Nakagawa *et al.* (2011) have suggested that this morphological change may be caused by depletion of cellular ATP and subsequent autophagosome formation [20,21]. The depletion of protons in the cellular by potent adsorption properties of $C_{60}$ may disturb the ATP synthesis in the mitochondria [24]. Additionally, there have been a few studies of mitochondrial damage caused by $C_{60}(OH)_x$ [21,22,25]. In this study, luminescence intensities associated with the ATP content of cells was measured. Low luminescence indicated the depletion of cellular ATP, reflecting functional damage of mitochondria and cell death. Furthermore, the WST-1 assay was used for evaluation of cytotoxicity, which is based on the content of dye produced by mitochondrial enzymes. Therefore, cell death and vacuole formation observed in dRLh-84 exposed to $C_{60}(OH)_{6-12}$ and $C_{60}(OH)_{12}$ may be caused by damage to mitochondrial functions (Figures 3 and 5).

Our results are in agreement with previous reports [21,22,25]. In addition, we have shown that $C_{60}(OH)_{6-12}$ and $C_{60}(OH)_{12}$ effectively caused more mitochondrial damage than other $C_{60}(OH)_x$ species in the liver cells.

## 4. Experimental Section

### *4.1. Chemicals*

Fullerene $C_{60}$ ($C_{60}$; nanom purple KN, purity > 99.9%) was purchased from Frontier Carbon Corporation (Fukuoka, Japan). $C_{60}(OH)_{n,\ n\ =\ 6-12}$ ($C_{60}(OH)_{6-12}$) was purchased from Kanto Chemical Co. Inc. (Tokyo, Japan). $C_{60}(OH)_2$ (purity of > 99%), $C_{60}(OH)_{12}$ pentahydrate, and $C_{60}(OH)_{36}$ octahydrate were purchased from FLOX Corporation (Kanagawa, Japan). With the exception of $C_{60}(OH)_2$, no information was available on the purity of the $C_{60}(OH)_x$ samples.

Mass spectrometric analysis of $C_{60}$ and $C_{60}(OH)_x$ was performed using LC-MS/MS (Waters Alliance 2695 HPLC system—Waters Micromass Quattro Micro API triple quadrupole mass spectrometer, Waters, Milford, USA).

### *4.2. Sample Preparation*

$C_{60}$ was ground in an agate mortar until the color of the powder changed to a brownish-black and was then suspended in dimethyl sulfoxide (DMSO) at a concentration of 10 mg/mL. The stock solution was sonicated and vortexed; and subsequently stored at −20 °C until being used. The $C_{60}$ solution was first diluted with DMSO; and subsequently diluted 100-fold with each growth medium before exposure to cells. $C_{60}(OH)_x$ were dissolved in DMSO at a concentration of 10 mg/mL; and were diluted in a manner similar to that used for $C_{60}$.

### *4.3. Cells*

Primary cultured rat hepatocytes and their culture medium were purchased from Biopredic International (Rennes, France). Rat hepatoma cells, dRLh-84, were obtained from the Health Science

Research Resources Bank (Osaka, Japan). HepG2 (Human hepatoma cells) were continuously cultured in our laboratory of National Institute of Health Sciences. HepG2 and dRLh-84 were grown in Eagle's minimum essential medium (MEM, Sigma-Aldrich, MO, USA), supplemented by 10% (v/v) fetal bovine serum (ICN Biochemicals Inc., OH, USA), 50 unit/mL penicillin and 50 μg/mL streptomycin (Gibco, CA, USA), 1 mM sodium pyruvate (Gibco, CA, USA), and 100 μM MEM non-essential amino acid (Gibco, CA, USA).

### *4.4. Cell Viability Assay*

Primary cells were seeded in 96-well plates at $0.3 \times 10^6$ cells/mL in 100 μL/well. dRLh-84 cells were seeded at $6 \times 10^3$ cells and HepG2 cells were seeded at $2 \times 10^4$ cells in 200 μL/well. The cells were incubated overnight at 37 °C in a humidified atmosphere containing 5% $CO_2$ in air, and then were exposed to test chemicals. After incubation for 3 days, cell viability was determined using the Cell Titer-Glo Luminescent Cell Viability Assay Kit (Promega, WI, USA). Since the luminescence intensity is based on the ATP content of viable cells, the luminescence intensity of each well was measured using a microplate reader (Mithras LB 940, Berthold technologies, Germany).

After dRLh-84 were exposed to 30 μg/mL of $C_{60}(OH)_{6-12}$ and $C_{60}(OH)_{12}$ for 24 h, cells were observed with the optical microscope and photographs of intracellular vacuoles were taken.

### *4.5. Mitochondrial Activity Assay*

Mitochondrial activity was measured using the Premix WST-1 kit (Takara, Tokyo, Japan). The absorbance of formazan dye was measured using a microplate reader (Ultraspec Visible Plate Reader II 96, GE Health, Buckinghamshire, UK) at a wavelength of 450 nm, with a reference wavelength of 620 nm. Measured using a microplate reader (Mithras LB 940, Berthold technologies, Germany).

### *4.6. Statistical Analysis*

Statistical analyses were performed using Student's *t*-test. The test was conducted to verify the difference between each group exposed to fullerenes and the control. Differences with $p < 0.05$ were considered statistical significant.

## 5. Conclusions

$C_{60}(OH)_{6-12}$ and $C_{60}(OH)_{12}$ showed higher levels of cytotoxicity in liver cells than $C_{60}$, $C_{60}(OH)_2$, and $C_{60}(OH)_{36}$, presumably due to mitochondrial damage. The number of hydroxyl group substituents on $C_{60}(OH)_x$ are an important factor in the determination of cytotoxic potential.

## Acknowledgments

This work was supported by a Research on Risk of Chemical Substances in Health and Labour Sciences Research Grant from the Ministry of Health, Labour, and Welfare of Japan.